J. Plasma Phys. (2018), *vol.* 84, 905840411
doi:10.1017/S0022377818000909

Transverse instability of electron phase-space holes in multi-dimensional Maxwellian plasmas

I. H. Hutchinson†

Plasma Science and Fusion Center, MIT, Cambridge, MA 02139, USA

(Received 21 April 2018; revised 6 August 2018; accepted 7 August 2018)

The stability of an initially one-dimensional electron hole to perturbations varying sinusoidally transverse to its trapping direction is analysed in detail. It is shown that the expected low-frequency eigenmode of the linearized Vlasov–Poisson system consists of a shift mode, proportional to the gradient of the equilibrium potential. The resulting dispersion relation is that the total jetting force exerted by a perturbed hole on the particles balances the electric restoring tension of the hole. The tension is quantitatively small and can often be ignored. The particle force is expressed as integrals of equilibrium parameters over the hole and is shown at low frequency to be exactly equal to what has recently been found (by different analysis) to express 'kinematic' hole momentum conservation. The mechanism of instability has nothing to do with the previously hypothesized transverse electron focusing. The unmagnetized growth rate $\gamma(k)$ is found numerically and is in excellent agreement with recent kinematic estimates. Magnetic field stabilization of the transverse mode is also evaluated. The resulting stability boundary for Maxwellian holes is in reasonable agreement with previously published criteria based on particle simulation. It arises from a change of trapped force sign across the resonance between bounce and cyclotron frequencies.

Key words: plasma instabilities, plasma nonlinear phenomena, space plasma physics

1. Introduction

An electron hole in a plasma is a solitary BGK mode (Bernstein, Greene & Kruskal 1957) consisting of a positive potential peak self-consistently maintained by phase-space density deficit of trapped electrons (Turikov 1984; Schamel 1986; Eliasson & Shukla 2006; Hutchinson 2017). In one dimension, electron holes are the normal nonlinear consequence of growth of an electrostatic instability driven by an unstable electron velocity distribution, for example a two-stream instability. However, it has been known since the earliest simulations (Morse & Nielson 1969) that in multiple dimensions electron holes either do not form or quickly break up by instability permitted by the additional dimensions; this is referred to as the transverse instability, and observed in many simulations since (Mottez *et al.* 1997; Miyake *et al.* 1998; Goldman, Oppenheim & Newman 1999; Oppenheim, Newman & Goldman 1999; Muschietti *et al.* 2000; Oppenheim *et al.* 2001; Singh, Loo & Wells 2001; Lu *et al.* 2008). Despite the obvious significance of this instability, since it determines

† Email address for correspondence: ihutch@mit.edu

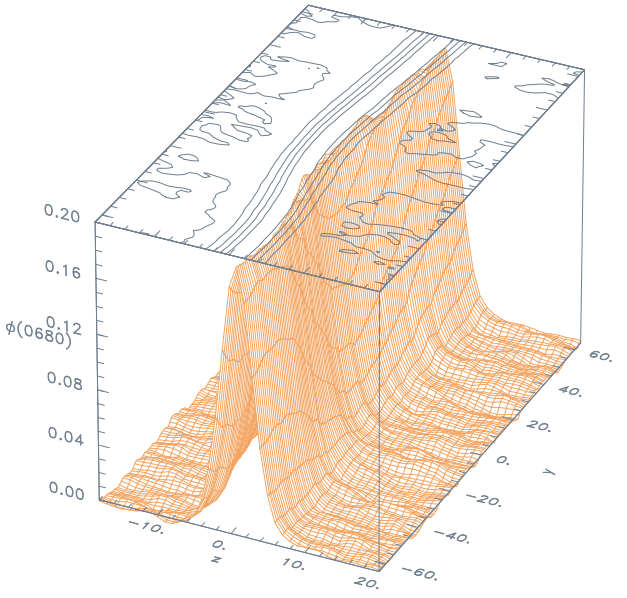

FIGURE 1. Two-dimensional (z, y) rendering and contours of potential ϕ of an initially one-dimensional hole in the early stages of a transverse instability in a particle-in-cell simulation.

the prevalence and fate of electron holes, satisfactory identification of its mechanism and rigorous analytical determination of its growth rate and threshold have until now been lacking. The current paper now presents this analysis.

Satellite measurements with high time resolution during the past 20 years have established (Matsumoto *et al.* 1994; Bale *et al.* 1998; Ergun *et al.* 1998; Mangeney *et al.* 1999; Pickett *et al.* 2008; Andersson *et al.* 2009; Wilson *et al.* 2010; Malaspina *et al.* 2013, 2014; Vasko *et al.* 2015; Mozer *et al.* 2016) that electron holes are widely present in a variety of space plasma regions. They are likely present also, though harder to resolve and observe, in many laboratory plasmas. Therefore it is increasingly pressing to develop a fundamental understanding of their persistence and stability.

Particle in cell (and some Vlasov continuum) simulations have been important in mapping out the phenomena. However, such simulations have not correctly identified the underlying instability mechanism. Figure 1 illustrates an example of a simulation, illustrating a hole and a growing kink in it. The natural idealization of the problem, concentrating on the stability properties rather than on hole formation, is to begin with a pre-formed hole (slab) equilibrium that varies in only one dimension. Simulations of this type have provided valuable insight (Muschietti *et al.* 1999, 2000; Wu *et al.* 2010), and identified the stabilizing effect of magnetic field. However the transverse 'focusing' mechanism, which they hypothesized causes the instability, is not confirmed either by subsequent simulations (Hutchinson 2018) or by the present analysis.

Analytic approaches to solving this linear stability problem have previously been at best only partly successful (Schamel 1982, 1987; Jovanović & Schamel 2002). A key difficulty lies in identifying the appropriate eigenmode structure in the direction of equilibrium non-uniformity (Lewis & Symon 1979). Previous unmagnetized analysis (Schamel 1982) made the inappropriate choice to address symmetric eigenmodes. It is shown here that, in agreement with simulations, the relevant eigenmode is

https://doi.org/10.1017/S0022377818000909 Published online by Cambridge University Press

predominantly antisymmetric. Another difficulty is to solve the linearized Vlasov equation by integration along characteristics in regimes that do not yield to simple expansions, in part because of non-uniformity. Previous analyses (Schamel 1982; Jovanović & Schamel 2002) have used expansion in inverse powers of frequency, which is inappropriate for these slowly (and purely) growing modes. The present study instead solves the Vlasov equation by numerical integration at finite complex frequency, showing excellent agreement at small ω with a better motivated analytic approximation. A previous study of magnetized holes (Jovanović & Schamel 2002) was, because of its expansions, limited to cases where the wave (ω) or cyclotron (Ω) frequencies are bigger than the highest bounce frequency of the trapped particles, yet concluded there was instability on the basis of a wave resonance $\omega + m\Omega \to 0$. The present study shows that the low-k transverse instability is stabilized when the cyclotron frequency exceeds the bounce frequency and that the wave frequency is always small, so there is no such resonance except $m = 0$ (which is effectively the one-dimensional case). Prior analytic studies provided no quantitative comparison with simulations. The present study gives quantitative predictions of the fastest growing mode and the previously proposed heuristic criterion (Miyake *et al.* 1998; Muschietti *et al.* 2000) for stabilization by magnetic field that agree well with simulations.

In view of these contrasts, a rather careful development of the mathematics is given here to provide rigor in the derivation, even though some of it has close parallels in the standard analysis of uniform equilibria. Section 2 gives the solution of the linearized Vlasov equation in terms of integrals along unperturbed orbits. Section 3 explains how the Poisson equation gives rise to a generalized eigen-problem and motivates its approximate solution in terms of conservation of momentum which is mathematically equivalent to a variational estimate of the eigenvalue for a shift mode perturbation. Section 4 derives the momentum conservation for unmagnetized plasmas and shows that it is in full agreement with a prior kinematic derivation. This leads to a simple analytic dispersion relation in the long-wavelength limit. Numerical integration at finite frequency gives the growth rate for all wavenumbers. Section 5 performs the analysis for plasmas with a magnetic field in the trapping direction and obtains the corresponding dispersion solutions, showing stabilization for Ω greater than bounce frequency.

The results are in full agreement with a more descriptive letter recently published by the author (Hutchinson 2018). The analysis provides the mathematical justification for the identification of the instability mechanism as being a kinematic one, arising from the transfer of momentum from hole potential to particles (Hutchinson & Zhou 2016; Zhou & Hutchinson 2016, 2017), called jetting.

2. Linearized Vlasov equation

Consider a localized positive potential peak equilibrium $\phi_0(z)$, the electron hole, to be analysed for linearized electrostatic perturbations. We address only the electron dynamics, taking the ions to be a uniform immobile background. We must retain full-wave treatment in the z-direction, but can Fourier analyse the transverse variation taking a transverse wavenumber k, without loss of generality in the y-direction. So the first-order potential perturbation is harmonic

$$\phi_1(\boldsymbol{x}, t) = \hat{\phi}(z) \exp \mathrm{i}(ky - \omega t). \tag{2.1}$$

Vlasov's equation is

$$\left(\frac{\partial}{\partial t} + \boldsymbol{v} \cdot \boldsymbol{\nabla} + \frac{q_e}{m_e} (\boldsymbol{E} + \boldsymbol{v} \wedge \boldsymbol{B}) \cdot \boldsymbol{\nabla}_v \right) f = 0. \tag{2.2}$$

https://doi.org/10.1017/S0022377818000909 Published online by Cambridge University Press

When linearized in an electrostatic approximation it becomes

$$\frac{\mathrm{d}f_1}{\mathrm{d}t} \equiv \left(\frac{\partial}{\partial t} + \boldsymbol{v}\cdot\boldsymbol{\nabla} + \frac{q_e}{m_e}(\boldsymbol{E}_0 + \boldsymbol{v}\wedge\boldsymbol{B}_0)\cdot\boldsymbol{\nabla}_v\right) f_1 = -\frac{q_e}{m_e}\boldsymbol{E}_1\cdot\boldsymbol{\nabla}_v f_0, \tag{2.3}$$

which is the rate of change of f_1 along the unperturbed orbit in phase space. And

$$\boldsymbol{E}_1 = -\boldsymbol{\nabla}\phi_1 = -\left(\frac{\partial\hat{\phi}}{\partial z}\boldsymbol{e}_z + \mathrm{i}k\hat{\phi}\boldsymbol{e}_y\right)\exp\mathrm{i}(ky-\omega t). \tag{2.4}$$

Integrating (2.3), we get the perturbed distribution:

$$f_1(\boldsymbol{v},\boldsymbol{x},t) = \frac{q_e}{m_e}\int_{-\infty}^{t}\left(\frac{\mathrm{d}\hat{\phi}}{\mathrm{d}z}\frac{\partial f_0}{\partial v_z} + \mathrm{i}k\hat{\phi}\frac{\partial f_0}{\partial v_y}\right)\exp\mathrm{i}(ky-\omega\tau)\,\mathrm{d}\tau, \tag{2.5}$$

where the integrand is to be evaluated on the unperturbed orbit, i.e. at $\boldsymbol{x}(\tau)$, $\boldsymbol{v}(\tau)$, which is the characteristic of the linearized equation.

The equilibrium distribution is a function of the constants of the unperturbed motion, which are the total parallel energy $W_\parallel = q_e\phi + m_e v_\parallel^2/2$ (with z the 'parallel' direction) and the perpendicular kinetic energy $W_\perp \equiv m_e v_\perp^2/2$. If a uniform background magnetic field, $B_0\boldsymbol{e}_z$ is present, then $v_\perp^2 = v_x^2 + v_y^2$, but if $B = 0$ we can interpret $v_\perp$ as v_y, and ignore v_x. So write

$$\frac{\partial f_0}{\partial v_z} = m_e v_z\frac{\partial f_0}{\partial W_\parallel}, \qquad \frac{\partial f_0}{\partial v_y} = m v_y\frac{\partial f_0}{\partial W_\perp}. \tag{2.6a,b}$$

And since $v_z(\mathrm{d}\hat{\phi}/\mathrm{d}z) = \mathrm{d}\hat{\phi}/\mathrm{d}\tau$,

$$f_1(\boldsymbol{v},\boldsymbol{x},t) = q_e\int_{-\infty}^{t}\left(\frac{\mathrm{d}\hat{\phi}}{\mathrm{d}\tau}\frac{\partial f_0}{\partial W_\parallel} + \mathrm{i}kv_y\hat{\phi}\frac{\partial f_0}{\partial W_\perp}\right)\exp\mathrm{i}(ky-\omega\tau)\,\mathrm{d}\tau. \tag{2.7}$$

The first term can be integrated by parts to give

$$f_1(t) = q_e\phi_1(t)\frac{\partial f_0}{\partial W_\parallel} + q_e\int_{-\infty}^{t}\left(\mathrm{i}(\omega-kv_y)\frac{\partial f_0}{\partial W_\parallel} + \mathrm{i}kv_y\frac{\partial f_0}{\partial W_\perp}\right)\hat{\phi}\mathrm{e}^{\mathrm{i}(ky-\omega\tau)}\,\mathrm{d}\tau, \tag{2.8}$$

assuming that $\phi_1(t=-\infty) = 0$. The leading term is then the 'adiabatic' response arising from the variation of a distribution that remains a constant function of total parallel energy $W_\parallel$ in response to a potential perturbation giving $\mathrm{d}W_\parallel = q_e\phi_1$. The integral term is the non-adiabatic response, which we shall denote $\tilde{f}$.

It is worth noticing that when the unperturbed distribution has a separable isotropic form in energy, for example on all passing orbits when the background is (isotropic) Maxwellian, the kv_y terms disappear because

$$-\frac{\partial f_0}{\partial W_\parallel} + \frac{\partial f_0}{\partial W_\perp} = 0. \tag{2.9}$$

But this happens only if the isotropy is in the hole's rest frame.

https://doi.org/10.1017/S0022377818000909 Published online by Cambridge University Press

3. The unstable shift eigenmode

3.1. *Eigen-analysis of the Poisson–Vlasov system*

The perturbed Poisson equation (leaving the factor $\mathrm{e}^{\mathrm{i}(ky-\omega t)}$ implicit) is

$$\nabla^2\phi_1 = \frac{\mathrm{d}^2\hat{\phi}}{\mathrm{d}z^2} - k^2\hat{\phi} = -\frac{q_e}{\epsilon_0}\int f_{\|1}\,\mathrm{d}v_z = -\frac{q_e}{\epsilon_0}\left(\hat{\phi}\frac{\mathrm{d}n_0}{\mathrm{d}\phi_0} + \int \tilde{f}_{\|}\,\mathrm{d}v_z\right). \tag{3.1}$$

The structure of the linear stability problem is then that we can regard the quantity $\tilde{n} = \int \tilde{f}_{\|}\,\mathrm{d}v_z$ as a linear functional of $\hat{\phi}$ determined by the solution of the linearized Vlasov equation. The Poisson equation for given k is then a generalized eigen-problem (Lewis & Symon 1979), of which the complex ω is effectively the eigenvalue and the spatial shape of $\hat{\phi}$ is the eigenmode. The non-uniformity of the equilibrium means that the eigenmode structure is of course not a Fourier mode. Determining all the eigenmodes and eigenvalues exactly is difficult, in part because $\tilde{n}$ is an integral, rather than differential, functional.

However, we are not attempting here to identify every mode; only the mechanism and growth rate of a specific type of perturbation observed to occur in simulations, namely the transverse instability. Therefore we concentrate on obtaining a good estimate of the eigenvalue, assuming we have a fair approximation to what the eigenmode shape is. For this purpose, we presuppose what characteristics of the eigenmode the simulations indicate, namely that it is present for small finite values of k (long transverse wavelength) and the magnitude of its complex frequency is small. To lowest order, then, the eigenmode equation can omit the terms $k^2\phi$ and $\tilde{n}$, in which case it must approximately satisfy

$$\frac{\mathrm{d}^2\hat{\phi}}{\mathrm{d}z^2} = -\frac{q_e}{\epsilon_0}\frac{\mathrm{d}n_0}{\mathrm{d}\phi_0}\hat{\phi} = \hat{\phi}\frac{\mathrm{d}}{\mathrm{d}\phi_0}\left(\frac{\mathrm{d}^2\phi_0}{\mathrm{d}z^2}\right). \tag{3.2}$$

It is easy to verify that this linear equation is satisfied by $\hat{\phi} = -\Delta(\mathrm{d}\phi_0/\mathrm{d}z)$, a shift mode, which is sometimes called the Goldston mode in soliton and other literature (see e.g. Skryabin (2002)). It consists of simply a displacement of the entire hole structure in the z-direction, which is obviously a neighbouring equilibrium, requiring no time derivative terms. In so far as there is a unique solution (modulo a position shift) for a BGK mode (electron hole) with specified distribution function, the shift appears to be the unique solution of this adiabatic equation. In any event, the simulations show that the mode does in fact consist predominantly of a shift, with some other minor distortions.

We then take advantage of the fact that an eigen-problem $\mathcal{L}\hat{\phi} = \lambda\mathcal{M}\hat{\phi}$ where $\mathcal{L}$ and $\mathcal{M}$ are self-adjoint operators[1], is equivalent to a variational problem that finds the extremum of the quotient $Q = \langle\hat{\phi}\mathcal{L}\hat{\phi}\rangle/\langle\hat{\phi}\mathcal{M}\hat{\phi}\rangle$, and that the eigenvalue therefore deviates from the quotient only by terms second order in any deviation of the $\hat{\phi}$ used in evaluating it from the exact eigenmode. Applying this approach we substitute the shift mode into the full Poisson equation, multiply by $\hat{\phi}$ and integrate over space. This process annihilates the adiabatic terms leaving

$$\Delta k^2\int \epsilon_0\left(\frac{\mathrm{d}\phi_0}{\mathrm{d}z}\right)^2\mathrm{d}z = -\int\frac{\mathrm{d}\phi_0}{\mathrm{d}z}q_e\int\tilde{f}_{\|}\,\mathrm{d}v_z\,\mathrm{d}z. \tag{3.3}$$

The value of ω that satisfies this equation is then anticipated to be a good approximation to the eigen-frequency of the mode.

[1] Schamel (1987) shows the present problem's operators are self-adjoint under some restrictions.

https://doi.org/10.1017/S0022377818000909 Published online by Cambridge University Press

3.2. *Force balance*

A simple physical interpretation of (3.3) is that it is the conservation of momentum: balancing the electric field tension (left-hand side) with the electric force on the non-adiabatic electron perturbation (right-hand side). That makes it an overall approximate 'kinematic' constraint. Indeed, this interpretation is one heuristic explanation of the transverse instability mechanism. It is a balance between the effects of 'jetting' – the momentum transfer to particles because of the acceleration of the hole (Hutchinson & Zhou 2016) – (right-hand side), and the stabilizing effects of electric field tension (left-hand side). We shall see shortly that in most circumstances the jetting is the predominant term and the stability boundary is approximately where the jetting is reduced to zero.

We can obtain this equation directly through force considerations without any immediate assumptions about the perturbation eigenmode shape, as follows. Force balance requires the total first-order (z-direction) force exerted by the electric field to be zero, because the electric field of a solitary potential structure is incapable of sustaining any net momentum transfer. Denoting the charge density by ρ, this is $E_0\rho_1$ plus $E_1\rho_0$ spatially integrated over the hole. These two forces (summed over species) are equal and opposite for a straight ($k=0$) isolated hole because,

$$\int \frac{\mathrm{d}\phi_0}{\mathrm{d}z}\frac{\rho_1}{\epsilon_0}\,\mathrm{d}z = -\int \frac{\mathrm{d}\phi_0}{\mathrm{d}z}\frac{\mathrm{d}^2\phi_1}{\mathrm{d}z^2}\,\mathrm{d}z = -\left[\frac{\mathrm{d}\phi_0}{\mathrm{d}z}\frac{\mathrm{d}\phi_1}{\mathrm{d}z}\right] + \int \frac{\mathrm{d}^2\phi_0}{\mathrm{d}z^2}\frac{\mathrm{d}\phi_1}{\mathrm{d}z}\,\mathrm{d}z = -\int \frac{\rho_0}{\epsilon_0}\frac{\mathrm{d}\phi_1}{\mathrm{d}z}\,\mathrm{d}z. \tag{3.4}$$

Integrating by parts the final form of (3.4) noting that ρ_0 is a function of ϕ_0, we find

$$\int \rho_0 \frac{\mathrm{d}\phi_1}{\mathrm{d}z}\,\mathrm{d}z = -\int \frac{\mathrm{d}\rho_0}{\mathrm{d}\phi_0}\frac{\mathrm{d}\phi_0}{\mathrm{d}z}\phi_1\,\mathrm{d}z. \tag{3.5}$$

A hole with y-variation ($k\neq 0$) has an additional term in ρ_1, arising from $\partial^2\phi_1/\partial y^2 = -k^2\phi_1$. Including it we get

$$\tilde{F} \equiv -\int \frac{\mathrm{d}\phi_0}{\mathrm{d}z}\left[\rho_1 - \frac{\mathrm{d}\rho_0}{\mathrm{d}\phi_0}\phi_1\right]\mathrm{d}z = -\epsilon_0 k^2 \int \frac{\mathrm{d}\phi_0}{\mathrm{d}z}\phi_1\,\mathrm{d}z \equiv F_E. \tag{3.6}$$

The term in the square brackets is manifestly the non-adiabatic charge density $q_e\tilde{n} = q_e\int \tilde{f}\,\mathrm{d}v$. Notice that because ϕ_0 is symmetric, this equation selects the antisymmetric part of ϕ_1. For a shift mode it is equivalent to the form $\int \phi_1^*\tilde{f}\,\mathrm{d}^3v\,\mathrm{d}^3x$ (whose variational Euler equation is the eigen-problem). The right-hand side becomes $F_E = \Delta k^2\int \epsilon_0(\mathrm{d}\phi_0/\mathrm{d}z)^2\,\mathrm{d}z$, which can be thought of as arising from the transfer of z-momentum in the y-direction via the electric field off-diagonal components of the Maxwell stress tensor $((\partial/\partial y)E_yE_z)$. It causes the hole to resist kinking as if it had a tension in the y-direction.

4. Unmagnetized plasmas

When there is no magnetic field, the transverse velocity v_y of the equilibrium (unperturbed) orbit is independent of time, and the τ dependence in the $\tilde{f}$ expression (2.8) resides only in $\hat{\phi}(z(\tau))$ and the exponent. In the τ-integral $y = y(\tau) = y(t) + v_y(\tau - t)$. We use time subscripts as shorthand for arguments ($y(t)\equiv y_t$ etc.)

https://doi.org/10.1017/S0022377818000909 Published online by Cambridge University Press

and $\omega' = \omega - kv_y$ to denote the frequency felt by the y-moving particle. Then we can write

$$\tilde{f} = \mathrm{i}q_e \left((\omega - kv_y) \frac{\partial f_0}{\partial W_\parallel} + kv_y \frac{\partial f_0}{\partial W_\perp} \right) \Phi \mathrm{e}^{\mathrm{i}(ky_t - \omega t)}, \tag{4.1}$$

where

$$\Phi(z_t) \equiv \int_{-\infty}^{t} \hat{\phi}(z(\tau)) \mathrm{e}^{-\mathrm{i}\omega'(\tau - t)} \, \mathrm{d}\tau, \tag{4.2}$$

which is independent of t, but not of the final position on the orbit z_t. All positions and velocities appearing here, and from now on, are for the unperturbed orbit.

4.1. *Shift mode perturbed distribution*

Now specialize to the case when the eigenmode is the shift mode $\hat{\phi}(z(\tau)) = -\Delta(\mathrm{d}\phi_0/\mathrm{d}z)$. Using

$$\frac{\mathrm{d}\phi_0}{\mathrm{d}z} = -\frac{m_e}{q_e} v_z \frac{\mathrm{d}v_z}{\mathrm{d}z} = -\frac{m_e}{q_e} \frac{\mathrm{d}v_z}{\mathrm{d}t}, \tag{4.3}$$

we have

$$\Phi = \Delta \frac{m_e}{q_e} \int_{-\infty}^{t} \frac{\mathrm{d}v_z}{\mathrm{d}\tau} \mathrm{e}^{-\mathrm{i}\omega'(\tau - t)} \, \mathrm{d}\tau = \Delta \frac{m_e}{q_e} \left\{ [v_z \mathrm{e}^{-\mathrm{i}\omega'(\tau - t)}]_{-\infty}^{\tau = t} + \int_{-\infty}^{t} v_z \mathrm{i}\omega' \mathrm{e}^{-\mathrm{i}\omega'(\tau - t)} \, \mathrm{d}\tau \right\}. \tag{4.4}$$

For a passing particle it is better to write v_∞ for the velocity at $\tau \to \pm\infty$ on the orbit under consideration and then $\mathrm{d}v_z/\mathrm{d}\tau = (\mathrm{d}/\mathrm{d}\tau)(v_z - v_\infty)$ so that

$$\Phi = \Delta \frac{m_e}{q_e} \left\{ (v_z(t) - v_\infty) + \int_{-\infty}^{t} (v_z - v_\infty) \mathrm{i}\omega' \mathrm{e}^{-\mathrm{i}\omega'(\tau - t)} \, \mathrm{d}\tau \right\}. \tag{4.5}$$

The advantage of this form is that $(v_z - v_\infty)$ is zero outside the hole so the integral has a finite domain. For trapped particles this same form applies provided that ω' has a positive imaginary part that ensures convergence and eliminates the lower limit contribution. Taking $v_\infty = 0$ is more convenient for trapped particles.

In any case, the first (integrated) term $(v_z - v_\infty)$ expresses the effect of an essentially rigid velocity shift of the trapped distribution function, because it gives rise to a term in $\tilde{f}$

$$m_e \mathrm{i}\omega' \Delta v_z \frac{\partial f_0}{\partial W_\parallel} = -m_e v_{\mathrm{hole}} v_z \frac{\partial f_0}{\partial W_\parallel} = -v_{\mathrm{hole}} \frac{\partial f_0}{\partial v_z}, \tag{4.6}$$

where $v_{\mathrm{hole}} = -\mathrm{i}\omega'\Delta = \dot{\Delta}$ is the hole incremental parallel velocity (observed in the v_y frame). The term involving $v_y(\partial f_0/\partial W_\perp) = \partial f_0/m_e \partial v_y$ is zero when integrated $\mathrm{d}v_y$.

A natural notation for the other term, because it has dimensions of velocity, is to denote it $\omega'\tilde{L}$ with

$$\tilde{L}(\omega') \equiv \int_{-\infty}^{t} (v_z - v_\infty) \mathrm{i} \mathrm{e}^{-\mathrm{i}\omega'(\tau - t)} \, \mathrm{d}\tau. \tag{4.7}$$

Although $\omega'\tilde{L}$ is locally of higher order in the transit time, it cannot be simply ignored at positions outside the hole, because all the other terms in Φ there are zero. It in fact gives rise to the net perturbation $\tilde{f}$ that crosses the outer boundary of the hole region. In other words, it is the source of the jetting perturbation. Besides which, when we are dealing with situations where ω' times the transit time is not small, the $\tilde{L}$ term contains all the resulting new behaviour, and it is the thing that is hard to calculate.

https://doi.org/10.1017/S0022377818000909 Published online by Cambridge University Press

4.2. *Shift mode rigid velocity shift contributes no force*

It is helpful to eliminate ϕ_0 from the shift mode expressions by using the orbit equilibrium relation equation (4.3), allowing us to express spatial variations in terms of v_z. It is also helpful for passing particles to transform distribution v_z-integrals into v_∞-integrals. Then at constant z (and ϕ)

$$v_\infty \,\mathrm{d}v_\infty = v_z \,\mathrm{d}v_z; \quad \text{so} \quad \frac{\partial v_z}{\partial v_\infty} = \frac{v_\infty}{v_z}. \tag{4.8}$$

Moreover, Vlasov's equation means $f_0(v_z) = f_\infty(v_\infty)$.

The non-adiabatic density perturbation $\tilde{n} = \int \tilde{f}\,\mathrm{d}^3v$ acquires a contribution $\tilde{n}_v$ from the first term $(v_z - v_\infty)$ of (4.5). However, its contribution to the total force (integrated over the hole) is zero because

$$\tilde{n}_v \equiv \int \mathrm{i}q_e\omega' \frac{\partial f_0}{\partial W_\parallel} \Delta \frac{m_e}{q_e}(v_z - v_\infty)\,\mathrm{d}^3v = \mathrm{i}\omega'\Delta \int \frac{\partial f_\infty}{\partial v_\infty}\left(1 - \frac{v_\infty}{v_z}\right)\mathrm{d}v_\infty; \tag{4.9}$$

and so

$$\begin{aligned}\tilde{F}_v \equiv \int -q_e \frac{\mathrm{d}\phi_0}{\mathrm{d}z}\tilde{n}_v \,\mathrm{d}z \;&=\; m_e \mathrm{i}\omega'\Delta \int\int v_z \frac{\mathrm{d}v_z}{\mathrm{d}z}\frac{\partial f_\infty}{\partial v_\infty}\left(1 - \frac{v_\infty}{v_z}\right)\mathrm{d}v_\infty\,\mathrm{d}z \\ &=\; m_e \mathrm{i}\omega'\Delta \int \frac{\partial f_\infty}{\partial v_\infty}\left[\int v_z\left(1 - \frac{v_\infty}{v_z}\right)\mathrm{d}v_z\right]\mathrm{d}v_\infty = 0. \end{aligned} \tag{4.10}$$

The same annihilation will occur for any quantity that can be rendered into the form of a spatial integral $(\mathrm{d}v_z/\mathrm{d}z)\mathrm{d}z \to \mathrm{d}v_z$ (the square bracket here, which is zero) when all the z-dependence of the integrand is in v_z. This proof is equally valid for trapped particles as for passing. Therefore for momentum balance purposes we can ignore $\tilde{F}_v$ and $\tilde{n}_v$.

The second term of equation (4.5), i.e. $\omega'\tilde{L}$, is not of this form and gives non-zero total force. From now on, we shall consider only shift modes and use Φ to denote just $\Delta(m_e/q_e)\omega'\tilde{L}$.

4.3. *Low-frequency jetting*

Major simplification of $\tilde{L}$ occurs for passing particles when ω' is much smaller than the inverse transit time of the particles through the hole, because then the $\mathrm{e}^{\mathrm{i}\omega'(\tau - t)}$ term can be taken to be unity. We defer integration $\mathrm{d}^2v_\perp$ over the perpendicular velocities and regard ω' as fixed for now. The resulting contribution[2] to the perturbed density from the $\partial f_0/\partial W_\parallel$ term is

$$\begin{aligned}\frac{\mathrm{d}\tilde{n}_p}{\mathrm{d}^2v_\perp} \;&=\; \int m_e \mathrm{i}\omega' \frac{\partial f_0}{\partial W_\parallel}\Delta \mathrm{i}\omega' \int_{z_s}^{z}(v_{z'} - v_\infty)\frac{\mathrm{d}z'}{v_{z'}}\,\mathrm{d}v_z \\ &=\; -\omega'^2\Delta \int \frac{\partial f_\infty}{\partial v_\infty}\int_{z_s}^{z}\left(1 - \frac{v_\infty}{v_{z'}}\right)\mathrm{d}z'\,\frac{\mathrm{d}v_\infty}{v_z}. \end{aligned} \tag{4.11}$$

[2]The notation $\mathrm{d}G/\mathrm{d}^2v_\perp$ denotes a quantity that when integrated $\mathrm{d}^2v_\perp$ gives G.

https://doi.org/10.1017/S0022377818000909 Published online by Cambridge University Press

Here the lower limit of the z'-integral z_s is the start of the orbit, which depends on the sign of v, which we will denote σ_v.[3] Contributions come only from places with $v_z \neq v_\infty$ i.e. $\phi \neq 0$, so $|z_s|$ must exceed the extent of the hole but need not actually be ∞. We denote the other end position of an entire spatial integral as z_f (finish of orbit).

The passing particle force is then

$$\begin{aligned}\frac{\mathrm{d}\tilde{F}_p}{\mathrm{d}^2 v_\perp} &= \sigma_v \int_{z_s}^{z_f} -q_e \frac{\mathrm{d}\phi_0}{\mathrm{d}z}\frac{\mathrm{d}\tilde{n}_p}{\mathrm{d}^2 v_\perp}\,\mathrm{d}z \\ &= -m_e\omega'^2\Delta\sigma_v \int_{z_s}^{z_f} v_z \frac{\mathrm{d}v_z}{\mathrm{d}z}\int \frac{\partial f_\infty}{\partial v_\infty}\int_{z_s}^{z}\left(1-\frac{v_\infty}{v_{z'}}\right)\mathrm{d}z'\frac{\mathrm{d}v_\infty}{v_z}\,\mathrm{d}z \\ &= -m_e\omega'^2\Delta\int \frac{\partial f_\infty}{\partial v_\infty}\sigma_v\int_{z_s}^{z_f}\frac{\mathrm{d}v_z}{\mathrm{d}z}\int_{z_s}^{z}\left(1-\frac{v_\infty}{v_{z'}}\right)\mathrm{d}z'\,\mathrm{d}z\,\mathrm{d}v_\infty. \end{aligned} \tag{4.12}$$

Now we do the $\mathrm{d}z$ integral by parts, making it

$$v_\infty\int_{z_s}^{z_f}\left(1-\frac{v_\infty}{v_{z'}}\right)\mathrm{d}z' - \int_{z_s}^{z_f} v_z\left(1-\frac{v_\infty}{v_z}\right)\mathrm{d}z = -\int_{z_s}^{z_f} v_z\left(1-\frac{v_\infty}{v_z}\right)^2\mathrm{d}z. \tag{4.13}$$

Reversing again the order of integration, we obtain a $\mathrm{d}v_\infty$ integral that can be done by parts

$$\int -\frac{\partial f_\infty}{\partial v_\infty} v_z\left(1-\frac{v_\infty}{v_z}\right)^2\mathrm{d}v_\infty = 2f_s v_{z0} + \int f_\infty \frac{d}{\mathrm{d}v_\infty}\left[v_z\left(1-\frac{v_\infty}{v_z}\right)^2\right]\mathrm{d}v_\infty, \tag{4.14}$$

where v_{z0} is the absolute value of v_z at the separatrix, and f_s is the distribution function on the separatrix. The leading term arises from the sign discontinuity of v_z at $v_\infty = 0$. Now

$$\begin{aligned}\frac{\mathrm{d}}{\mathrm{d}v_\infty}\left[v_z\left(1-\frac{v_\infty}{v_z}\right)^2\right] &= \left[\frac{v_\infty}{v_z}\left(1-\frac{v_\infty}{v_z}\right) - 2\left(1-\frac{v_\infty^2}{v_z^2}\right)\right]\left(1-\frac{v_\infty}{v_z}\right) \\ &= -2+3\frac{v_\infty}{v_z}-\frac{v_\infty^3}{v_z^3}. \end{aligned} \tag{4.15}$$

Hence

$$\frac{\mathrm{d}\tilde{F}_p}{\mathrm{d}^2 v_\perp} = -m_e\omega'^2\Delta\left\{\sigma_v\int_{z_s}^{z_f} 2f_s v_{z0} + \int\left[-2+3\frac{v_\infty}{v_z}-\left(\frac{v_\infty}{v_z}\right)^3\right]f_\infty\,\mathrm{d}v_\infty\,\mathrm{d}z\right\}, \tag{4.16}$$

where $\sigma_v\int_{z_s}^{z_f}\mathrm{d}z$ is simply $\int\mathrm{d}z$. This agrees[4] with the prior kinematic calculation (Hutchinson & Zhou 2016), except for the presence of the term $2f_s v_{z0}$.

The trapped particle contribution associated with $\partial f/\partial W_\parallel$ can be treated using the same sequence of partial integrations except that the $v_\infty = 0$ choice means we cannot

[3]Consequently, for negative v_∞, $\mathrm{d}z'$ is negative, but $\mathrm{d}z'/v_z$ is positive, as is $\mathrm{d}v_\infty$. Thus for opposite signs of $\partial f_\infty/\partial v_\infty$, the density perturbations arising from opposite velocities are opposite. They are also on opposite sides of the hole; so when multiplied by the antisymmetric potential gradient, opposite velocities give jetting force in the same direction.

[4]Since $-\omega^2\Delta = (\mathrm{i}\omega)^2\Delta = \ddot{\Delta}$ which is the hole acceleration.

https://doi.org/10.1017/S0022377818000909 Published online by Cambridge University Press

adopt v_∞ as the velocity integration variable. The past orbit integral now extends to $\tau = -\infty$, because the orbit never escapes the hole, but assuming ω to have a positive imaginary part, the integral converges and the lower limit can be ignored[5]. The phase-space element $(\partial f/\partial W_\parallel)\mathrm{d}W_\parallel = (\partial f/\partial v_z)\,\mathrm{d}v_z$ commutes with the $\mathrm{d}z$ integral. We interpret $\mathrm{d}W_\parallel$ as implying summing over positive and negative velocities, so we can consider the $\mathrm{d}z$ integral to be over the entire relevant orbit range in the positive direction (avoiding the need for σ_v).

$$\begin{aligned}\frac{\mathrm{d}\tilde{F}_t}{\mathrm{d}^2 v_\perp} &= m_e \Delta \int v_z \frac{\mathrm{d}v_z}{\mathrm{d}z} \int \mathrm{i}\omega' \frac{\partial f_0}{\partial v_z} \mathrm{i}\omega' \int_{z_s}^{z} \mathrm{d}z' \frac{\mathrm{d}v_z}{v_z}\,\mathrm{d}z \\ &= -m_e \omega'^2 \Delta \int \frac{\partial f_0}{\partial v_z} \int \frac{\mathrm{d}v_z}{\mathrm{d}z} \int_{z_s}^{z} \mathrm{d}z'\,\mathrm{d}z\,\mathrm{d}v_z. \\ &= m_e \omega'^2 \Delta \int \frac{\partial f_0}{\partial v_z} \int v_z\,\mathrm{d}z\,\mathrm{d}v_z = m_e \omega'^2 \Delta \int \int \frac{\partial f_0}{\partial v_z} v_z\,\mathrm{d}v_z\,\mathrm{d}z \\ &= m_e \omega'^2 \Delta \int \left[2 f_s v_{z0} - \int_{-v_{z0}}^{v_{z0}} f_0\,\mathrm{d}v_z \right] \mathrm{d}z. \end{aligned} \tag{4.17}$$

The term $2f_s v_{z0}$, which arises from the limits of integration $\mathrm{d}v_z$ at the separatrix, cancels the similar term in the passing particle force expression (4.16). Without that term, the trapped force can be considered to be simply the inertia of the trapped particles.

When $k = 0$, $\omega' = \omega$, we can integrate $\mathrm{d}^2 v_\perp$, and no $\partial f/\partial W_\perp$ term need be considered. Then we find

$$\tilde{F} = \tilde{F}_p + \tilde{F}_t = m_e \ddot{\Delta} \int_{z_s}^{z_f} \left\{ \int \left[-2 + 3\frac{v_\infty}{v_z} - \left(\frac{v_\infty}{v_z}\right)^3 \right] f_\infty\,\mathrm{d}v_\infty + \int_{-v_{z0}}^{v_{z0}} f\,\mathrm{d}v_z \right\} \mathrm{d}z, \tag{4.18}$$

where f here is the (unperturbed) one-dimensional (v_z)-distribution function. This force expression is in full agreement with the prior one-dimensional kinematic calculation (Hutchinson & Zhou 2016).

We observe that since an electron hole has no net electric charge, for immobile ions the sum of the trapped electron charge and the integrated difference of the passing electron charge density from its external value must be zero. This allows us to deduce an alternative expression for the trapped particle number:

$$\int_{z_s}^{z_f} \int_{-v_{z0}}^{v_{z0}} f\,\mathrm{d}v_z\,\mathrm{d}z = \int_{z_s}^{z_f} \int \left(1 - \left|\frac{v_\infty}{v_z}\right|\right) f_\infty\,\mathrm{d}v_\infty\,\mathrm{d}z. \tag{4.19}$$

4.4. *Low-frequency momentum balance including $\partial f/\partial W_\perp$ terms*

Let us suppose that the external distribution is isotropic Maxwellian (and the hole is stationary in the Maxwellian frame). Then the kv_y terms in $\tilde{f}$ cancel each other for passing particles which has the effect of making one of the ω' terms in equation (4.16) just ω. No such cancellation occurs for the trapped particles because the sign of $\mathrm{d}f/\mathrm{d}W_\parallel$ is reversed: the electron distribution is smaller at smaller v_z. For shallow holes

[5]The orbit integral is written in (4.17) in terms of $\mathrm{d}z' = v_z'\,\mathrm{d}\tau$. The start of the orbit z_s is taken sufficiently far back in time that the perturbing potential is negligible then, and since the z' excursion in space is bounded for trapped orbits, we can ignore the lower limit.

https://doi.org/10.1017/S0022377818000909 Published online by Cambridge University Press

for trapped particles $|\mathrm{d}f/\mathrm{d}W_\parallel| \gg |\mathrm{d}f/\mathrm{d}W_\perp|$ so the $\mathrm{d}f/\mathrm{d}W_\perp$ term hardly contributes. A simple way to account for it is to suppose that the distribution is of the Schamel type (Schamel 1979) having a parallel Maxwellian of negative temperature in the trapped region. In that case,

$$\frac{\partial f}{\partial W_\parallel} = \beta \frac{\partial f}{\partial W_\perp}, \tag{4.20}$$

where β is the inverse of the ratio (a negative quantity) of trapped parallel temperature to perpendicular. This ansatz is very convenient because it allows us simply to multiply $kv_y(\partial f/\partial W_\parallel)$ by $(1 + 1/|\beta|)$ to account for the $\partial f/\partial W_\perp$ term. This extra factor accompanies all k^2 terms. For a slow-moving hole, $-\beta \approx 1 + (15/16)\sqrt{\pi T_e/e\psi}$, which is large for a shallow hole (small ψ). But the quantity $1/|\beta| \approx 0.346$ is still only a moderate correction for a deep hole $\psi = T_e/e$.

We still need to integrate over v_y to arrive at the total force. When we do so, first-order kv_y terms coming from the cross-products $\omega k v_y$ integrate to zero for a symmetric $f(v_y)$ distribution. The passing particle force $\tilde{F}_p$ then is unchanged in form except that only ω appears in it, not ω'. The trapped force $\tilde{F}_t$ has an ω^2 term that adds to the passing as before, plus a $k^2\langle v_y^2\rangle$ term that is otherwise of the same form as (4.17).

Consequently, using $\langle v_y^2\rangle = T_y/m_e$, and considering f to be the parallel distribution function, the full particle force can be taken as

$$\begin{aligned}\tilde{F} &= -m_e\Delta \int \omega^2 \left\{ \int \left[-2 + 3\frac{v_\infty}{v_z} - \left(\frac{v_\infty}{v_z}\right)^3 \right] f_\infty \,\mathrm{d}v_\infty + \int_{-v_{z0}}^{v_{z0}} f \,\mathrm{d}v_z \right\} \\ &\quad + \left(1 + \frac{1}{|\beta|}\right) k^2 \frac{T_y}{m_e} \left\{ -2v_s f_s + \int_{-v_{z0}}^{v_{z0}} f \,\mathrm{d}v_z \right\} \mathrm{d}z. \end{aligned} \tag{4.21}$$

$$\begin{aligned} &= -m_e\Delta \int \omega^2 \left\{ \int \left[-1 + 2\frac{v_\infty}{v_z} - \left(\frac{v_\infty}{v_z}\right)^3 \right] f_\infty \,\mathrm{d}v_\infty \right\} \\ &\quad + \left(1 + \frac{1}{|\beta|}\right) k^2 \frac{T_y}{m_e} \left\{ \int_{-v_{z0}}^{v_{z0}} (f - f_s) \,\mathrm{d}v_z \right\} \mathrm{d}z \\ &= m_e \Delta n_\infty \int \left[\omega^2 h(\chi) + \left(1 + \frac{1}{|\beta|}\right) k^2 \frac{T_y}{m_e} g(\chi) \right] \mathrm{d}z. \end{aligned} \tag{4.22}$$

The curly brace expressions have been denoted by the dimensionless functions h and g, which depend upon potential ϕ expressed in terms of $\chi^2 = -q_e\phi/T_e = m_e v_{z0}^2/2T_e$. They are both positive. In so far as the electric field stress is negligible, the dispersion relation is $\tilde{F} = 0$ which immediately shows that $\omega^2 = -(\langle g\rangle/\langle h\rangle)(1 + 1/|\beta|)k^2 T_y/m_e$, where $\langle g\rangle$ and $\langle h\rangle$ are the spatial averages of g and h. The frequency is therefore pure imaginary, one root being positive, which is a growing unstable perturbation.

For an unshifted Maxwellian f_∞, the velocity integrals needed for (4.22) can be carried out. They are

$$h(\chi) = -2\int_0^\infty \left[-1 + 2\frac{v_\infty}{v_z} - \left(\frac{v_\infty}{v_z}\right)^3 \right] \frac{f_\infty}{n_\infty} \,\mathrm{d}v_\infty = -\frac{2}{\sqrt{\pi}}\chi + (2\chi^2 - 1)\mathrm{e}^{\chi^2}\,\mathrm{erfc}(\chi) + 1, \tag{4.23}$$

and (using (4.19))

$$g(\chi) = 2\left\{ \frac{f_s}{n_\infty} v_{z0} - \int_0^\infty \left(\frac{1 - v_\infty}{v_z}\right) \frac{f_\infty}{n_\infty} \,\mathrm{d}v_\infty \right\} = \frac{2}{\sqrt{\pi}}\chi - [1 - \mathrm{e}^{\chi^2}\,\mathrm{erfc}(\chi)]. \tag{4.24}$$

https://doi.org/10.1017/S0022377818000909 Published online by Cambridge University Press

For small χ the power series is $\mathrm{erfc}(\chi) = 1 - (2/\sqrt{\pi})[\chi - \chi^3/3 + O(\chi^5)]$, so $h(\chi) = \chi^2 - (2/\sqrt{\pi})(4/3)\chi^3 + O(\chi^4)$ and $g(\chi) = \chi^2 - (2/\sqrt{\pi})(2/3)\chi^3 + O(\chi^4)$. The ratio $g/h \to 1$ as $\chi \to 0$; at $\chi = 1$, $g/h = 1.86$ and $\langle g\rangle/\langle h\rangle = 1.63$ (for a $\mathrm{sech}^4 z$ shape potential).

The electric tension force when $\phi_0 = \psi\,\mathrm{sech}^4(z/4\lambda_D)$ can be evaluated as

$$F_E = \Delta\epsilon_0 k^2 \int \left(\frac{\mathrm{d}\phi_0}{\mathrm{d}z}\right)^2 \mathrm{d}z = \Delta\epsilon_0 k^2 \frac{\psi^2}{\lambda_D}\frac{128}{315} = \Delta k^2 \lambda_D \frac{q_e^2\psi^2 n_\infty}{T_e}\frac{128}{315}. \tag{4.25}$$

Therefore the full dispersion relation is

$$m_e\omega^2 \int h(\chi)\,\mathrm{d}z = -k^2 T_y \left(\left(1 + \frac{1}{|\beta|}\right)\int g(\chi)\,\mathrm{d}z - \lambda_D \frac{q_e^2\psi^2}{T_y T_e}\frac{128}{315}\right). \tag{4.26}$$

A crucial observation is that as $\psi \to 0$, g, $h \to \chi^2 \sim \psi$, whereas the electric tension scales like ψ^2. Therefore for shallow holes ($\psi \ll eT_e$) the F_E term is ignorable. Even for a deep hole such as $\psi = eT_e$, numerical evaluation shows that $\int g(\chi)\,\mathrm{d}z = 0.55 \times 4\lambda_D$, which makes the g term 5.4 times larger than F_E. Therefore, for all but exceptionally deep holes, F_E can be ignored for low-k modes.

In summary then, ignoring F_E, the predicted instability at low k, where the transit, or bounce, time of the electrons is short compared with $1/\omega'$, is that the imaginary part of the frequency is

$$\omega_i = k\sqrt{\frac{T_y}{m_e}}\sqrt{\frac{\langle g\rangle}{\langle h\rangle}\left(1 + \frac{1}{|\beta|}\right)} \tag{4.27}$$

where the second square root factor is unity for shallow holes and rises only to 1.48 for $\psi \simeq T_e/e$. (The real part of the frequency is zero.)

In view of the proportionality of ω_i and k, one expects that the fastest growing mode has large k. However, the calculation so far is for low-k. Therefore the observed growth rate in a simulation or in nature is anticipated to be at the upper end of the k-range for which the low-k approximations apply. We therefore need to analyse the breakdown of the low-k approximations, to find the behaviour of the fastest growing modes.

4.5. *Full dispersion relation including finite transit time effects*

In order to determine the behaviour at high-k near the instability threshold, we must consider situations where the transit time is comparable to $1/\omega'$. We must therefore abandon the low-k approximation and fully account for ω' in the integral $\tilde{L}$ in (4.7). Rather than pursue further analytical approximation, numerical integration is adopted. Since this requires a quadruple integration over τ, v_y, v_z and z, which becomes computationally expensive if not done efficiently, it is helpful to recognize that one can actually combine the evaluations corresponding to all positions z into a single orbit integral $\mathrm{d}\tau$. In other words, one does not have to do a different orbit integral for every position z for a certain parallel energy v_z^2. That integral can be done once, accumulating values for all positions z and can be scaled to provide $\tilde{L}$, Φ and hence $\tilde{f}$ and the force contribution.

https://doi.org/10.1017/S0022377818000909 Published online by Cambridge University Press

4.5.1. *Evaluation of the past orbit integral for passing particles*

For passing particles of specified v_∞, we perform spatial integrals on a uniform z-grid, starting at a negative z position z_s far enough outside the hole to have its integrand negligible. Call the past orbit time there $\tau_s = 0$. For each succeeding position $z_j = z_s + j\delta z$, we find its corresponding orbit time as $\tau_{j+1} - \tau_j = \delta\tau = \delta z(1/v_j + 1/v_{j+1})/2$ which is an appropriate trapezoid increment for $\tau = \int \mathrm{d}z/v$. The v_j depend only on the known potential ϕ_j at z_j, and on v_∞. The next value of $\tilde{L} \equiv \int_{\tau_s}^{t} (v - v_\infty)\mathrm{i}\mathrm{e}^{-\mathrm{i}\omega'(\tau - t)}\,\mathrm{d}\tau$ is calculated writing $v_{j+1/2} = (v_{j+1} + v_j)/2$ and using

$$\begin{aligned}\tilde{L}_{j+1} - \mathrm{e}^{\mathrm{i}\omega'\delta\tau}\tilde{L}_j \;&\approx\; (v_{j+1/2} - v_\infty)\int_{\tau_j}^{\tau_{j+1}} \mathrm{i}\mathrm{e}^{-\mathrm{i}\omega'(\tau - \tau_{j+1})}\,\mathrm{d}\tau \\ &=\; -(v_{j+1/2} - v_\infty)\frac{1}{\omega'}[1 - \mathrm{e}^{\mathrm{i}\omega'\delta\tau}]. \end{aligned} \tag{4.28}$$

This approach preserves accuracy since v is slowly varying even if $\mathrm{e}^{-\mathrm{i}\omega'\tau}$ is not. Thus all values of $\tilde{L}_j$ and hence of Φ (4.5) and the contribution to the hole force on the entire uniform z-mesh are obtained from one cumulative integral procedure, that gives

$$\frac{\mathrm{d}F_p}{\mathrm{d}^2 v_\perp \mathrm{d}v_\infty} = \mathrm{i}m_e\Delta\left(\omega'\frac{\partial f_0}{\partial W_\parallel} + (\omega - \omega')\frac{\partial f_0}{\partial W_\perp}\right)\int -q_e\frac{\mathrm{d}\phi}{\mathrm{d}z}\omega'\tilde{L}(z, \omega')\frac{\mathrm{d}z}{v_z}v_\infty, \tag{4.29}$$

which can then be integrated over the (passing) velocity v_∞ and v_y (and trivially v_x).

4.5.2. *Evaluation of the past orbit integral for trapped particles*

For trapped particles take $v_\infty = 0$ and then denote orbits instead by the quantity $v_\psi = \sqrt{2(-q_e\psi + W_\parallel)/m_e} > 0$, which is the orbit speed at $z = 0$, $\phi = \psi$, when the parallel energy is the negative quantity $W_\parallel (\geqslant q_e\psi)$. To obtain high resolution near the separatrix, it is best to space orbits by equal intervals of $\sqrt{-W_\parallel}$. For a given v_ψ the orbit has a finite z-extent, and turning points ($v_z = 0$) at its ends. Equally spaced z-positions are used, but spanning just the z-extent of the orbit (different for each energy $W_\parallel$). Near the ends of the orbit, integration interpolation is optimized by determining $\delta\tau$ via $\delta t = \delta v/\dot{v}$; but near $z = 0$ using $\delta t = \delta z/v$ is better. Again τ integrals are combined with z-integrals over the hole's spatial extent, by making the v_y integral the outermost and converting the combined $\mathrm{d}v_\psi \mathrm{d}z$ phase-space integral of the orbit contribution over the entire hole into an equivalent $\mathrm{d}\tau$ integral round the closed phase-space orbit. Schematically $F_t = \int \ldots \mathrm{d}\tau'\,\mathrm{d}z\,\mathrm{d}v_z\mathrm{d}v_y = \int \ldots \mathrm{d}\tau'\,\mathrm{d}\tau\,v_\psi\,\mathrm{d}v_\psi\,\mathrm{d}v_y$.[6]

As previously noted, one must assume that ω' has a positive imaginary part ω_i which ensures the backward τ integral giving $\tilde{L}$ converges. But it is obvious that the contribution from each preceding orbit period is the same except that they are multiplied by successive factors $\exp(\mathrm{i}\omega' t_b)$, where t_b is the orbit (bounce) period. This factor accounts for the attenuation $\exp(\omega_i\tau)$ and the phase change relative to the succeeding period. Therefore it is necessary to perform the integral numerically only

[6]The integral over phase space between two orbits may be written $\int\int \mathrm{d}z\,\mathrm{d}v_z = \int\int \mathrm{d}\tau\,v_\psi\,\mathrm{d}v_\psi$, because by the incompressibility of phase-space flow, the normal distance between adjacent orbits is $\mathrm{d}v_\psi s_\psi/s$ where $s = \sqrt{v_z^2 + (\mathrm{d}v_z/\mathrm{d}t)^2}$ is the speed of phase-space motion and $s_\psi = v_\psi$ (at the well centre $\phi = \psi$ where $\mathrm{d}v_z/\mathrm{d}t = 0$), so $\mathrm{d}v\,\mathrm{d}z \to s\,\mathrm{d}\tau\,\mathrm{d}v_\psi s_\psi/s = v_\psi\,\mathrm{d}\tau\,\mathrm{d}v_\psi$.

https://doi.org/10.1017/S0022377818000909 Published online by Cambridge University Press

around a single period of the orbit; the total including all the prior periods can then be synthesized by multiplying by the infinite sum[7]:

$$\sum_{\ell=0}^{\infty}[\exp(\mathrm{i}\omega' t_b)]^{\ell} = 1/[1-\exp(\mathrm{i}\omega' t_b)]. \tag{4.30}$$

It does not matter where one chooses to start and stop the single orbit numerically evaluated. For definiteness, choose to start the integral at $\tau = 0$ saving the cumulative integral $L(t) = \int_0^t v_z \mathrm{i} e^{-\mathrm{i}\omega'(\tau - t)}\,\mathrm{d}\tau$. Then take $\tau = 0$ to be the left end of the orbit (where v_z changes sign from negative to positive). To construct the first prior orbit for any other position z, v_z on it, take t to be the value of τ during the first orbit at which the numerically calculated orbit passes through that position.

Since the hole is reflectionally symmetric, it suffices to calculate only half of the orbit, where $0 < t \leqslant t_b/2$. Starting at the left-hand end and integrating up to the right-hand end is the same as starting at the right and integrating along the negative-v part of the orbit to the left. The only difference is that the velocity is opposite in sign. The resulting reversal of Φ is cancelled by the reflection of the z position and the consequent reversal of $\mathrm{d}\phi_0/\mathrm{d}z$. Hence positive and negative velocity parts of the integral give equal contribution to the force. The complete integral for a full prior period ending in the $0 < t \leqslant t_b/2$ segment is obtained as the sum of four parts of the orbit: $(0 \to t)$, $(t - t_b \to -t_b/2)$, $(-t_b/2 \to -t_b/2 + t)$, $(-t_b/2 + t \to 0)$. Noting that $\int_{-t_b}^{t-t_b} v_z \mathrm{i} e^{-\mathrm{i}\omega'(\tau - t)}\,\mathrm{d}\tau = e^{\mathrm{i}\omega' t_b} L(t)$, $\int_{-t_b/2}^{t-t_b/2} v_z \mathrm{i} e^{-\mathrm{i}\omega'(\tau - t)}\,\mathrm{d}\tau = -e^{\mathrm{i}\omega' t_b/2} L(t)$ and $\int_t^{t_b/2} v_z \mathrm{i} e^{-\mathrm{i}\omega'(\tau - t)}\,\mathrm{d}\tau = e^{\mathrm{i}\omega'(t - t_b/2)} L(t_b/2) - L(t)$ one finds

$$\begin{aligned}
\int_{t-t_b}^{t} v_z(\tau)\mathrm{i} e^{-\mathrm{i}\omega'(\tau - t)}\,\mathrm{d}\tau &= \int_0^t + \int_{t-t_b}^{-t_b/2} + \int_{-t_b/2}^{-t_b/2+t} + \int_{-t_b/2+t}^{0} v_z(\tau)\mathrm{i} e^{-\mathrm{i}\omega'(\tau - t)}\,\mathrm{d}\tau \\
&= L(t) + e^{\mathrm{i}\omega' t_b}[e^{\mathrm{i}\omega'(t - t_b/2)} L(t_b/2) - L(t)] \\
&\quad - e^{\mathrm{i}\omega' t_b/2} L(t) - e^{\mathrm{i}\omega' t_b/2}[e^{\mathrm{i}\omega'(t - t_b/2)} L(t_b/2) - L(t)] \\
&= (1 - e^{\mathrm{i}\omega' t_b}) L(t) + e^{\mathrm{i}\omega' t}(e^{\mathrm{i}\omega' t_b/2} - 1) L(t_b/2).
\end{aligned} \tag{4.31}$$

And the full prior time integral from $-\infty$ to give $\tilde{L}$ is obtained by multiplying by (4.30).

Then

$$\frac{\mathrm{d}F_t}{\mathrm{d}^2 v_\perp \mathrm{d}v_\psi} = \mathrm{i} m_e \Delta \left(\omega' \frac{\partial f_0}{\partial W_\parallel} + (\omega - \omega') \frac{\partial f_0}{\partial W_\perp} \right) \int -q_e \frac{\mathrm{d}\phi}{\mathrm{d}z} \omega' \tilde{L}(z, \omega') \frac{\mathrm{d}z}{v_z} v_\psi, \tag{4.32}$$

where the integral $\mathrm{d}z/v_z = \mathrm{d}t$ is over the half-orbit with positive v_ψ, and an equal contribution also comes from the negative-v_ψ half.

4.5.3. *Results*

Implementing these algorithms gives the forces F_t and F_p for specified general values of ψ, k and ω for some specified potential form $\phi_0(z)$ and distribution function f. A verification of the numerics is obtained by comparing the values found at $k = 0$, $\mathrm{Re}(\omega) = 0$, and $\mathrm{Im}(\omega)$ small, with the analytic expressions leading up to equation (4.18), and employing the forms (4.23) and (4.24).

[7]This is a much more satisfactory numerical approach for the anharmonic orbits of a hole than expanding the motion as an infinite Fourier series. It retains the resonant behaviour of the response, as can be seen by the fact that the denominator goes to zero where $\omega' t_b = 2\pi n$. See Lewis & Seyler (1982) for a formal discussion of this sort of expression.

https://doi.org/10.1017/S0022377818000909 Published online by Cambridge University Press

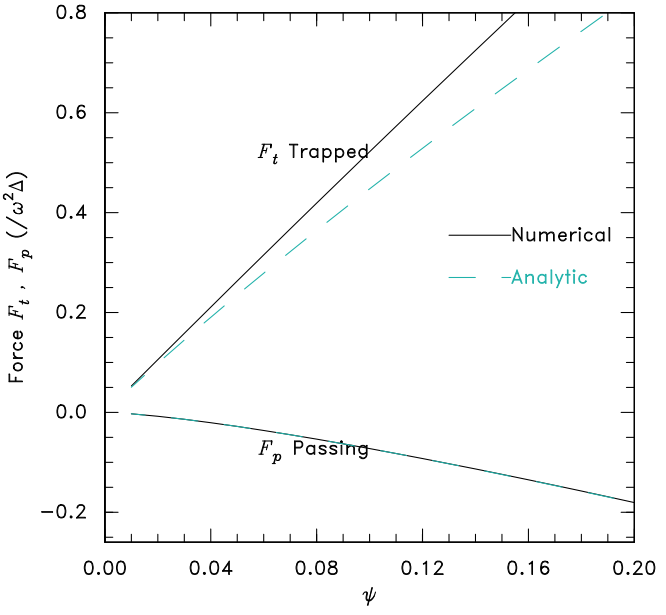

FIGURE 2. Comparison of numerical and analytic calculations of trapped and passing particle forces, for small value of ω_i and zero k and ω_r. The forces are real for symmetric v_y-distributions. (ψ is measured in units of T_e/e.)

As figure 2 indicates, we find essentially exact agreement for the passing particle force F_p, using Maxwellian distributions and a potential $\phi = \psi\,\mathrm{sech}^4(z/4)$ at all values of ψ. However, the trapped particle force requires a self-consistent parallel velocity distribution, which is not readily available analytically except for shallow holes. Using the approximation $f(W_\parallel) = f_\infty(0)\exp(-\beta W_\parallel)$ with $-\beta = 1 + (15/16)\sqrt{\pi T_e/e\psi}$, better than 2 % agreement in F_t is obtained for $\psi < 0.02$, which verifies the integration coding.

As k is increased from zero the main effect is observed to occur as a reduction of F_t, with only small changes to F_p. In figure 3 is shown the total particle force and the electric tension force as a function of k for two (fixed) imaginary frequencies $\omega = i\omega_i$. It illustrates the fact that the tension force F_E (drawn for the corresponding ψ values and varying $\propto \psi^2$) is a minor correction, probably less important in practice than the approximation arising from taking the trapped distribution to be $\propto \exp(-\beta v_z^2)$. For small ω_i (figure 3*a*), this plot is essentially universal. It gives the small-k dispersion root at the intersection of corresponding curves, where kv_t/ω_i is slightly below 1 in accordance with (4.27). However for larger ω_i and correspondingly kv_t (figure 3*b*), there is no intersection for shallow holes (small ψ) because the curves of $F_t + F_p$ have a minimum above zero. Figure 3(*b*) also illustrates the existence of a second solution at higher k for higher ψ values. We shall shortly see that this behaviour arises because of changes of resonance on trapped electrons.

The dispersion relation that solves $F_t + F_p = F_E$ can usefully be displayed in terms of $\gamma \equiv \omega_i$ as a function of given k. This can be accomplished for a stationary hole in a Maxwellian distribution by bisection real root finding because the real part of ω is zero by symmetry. Both k and γ scale like $\sqrt{\psi}$, so plotting the resulting $\gamma/\sqrt{\psi}$ versus $k/\sqrt{\psi}$, as shown in figure 4, gives an almost universal curve, at least for $\psi \lesssim 0.5$.

https://doi.org/10.1017/S0022377818000909 Published online by Cambridge University Press

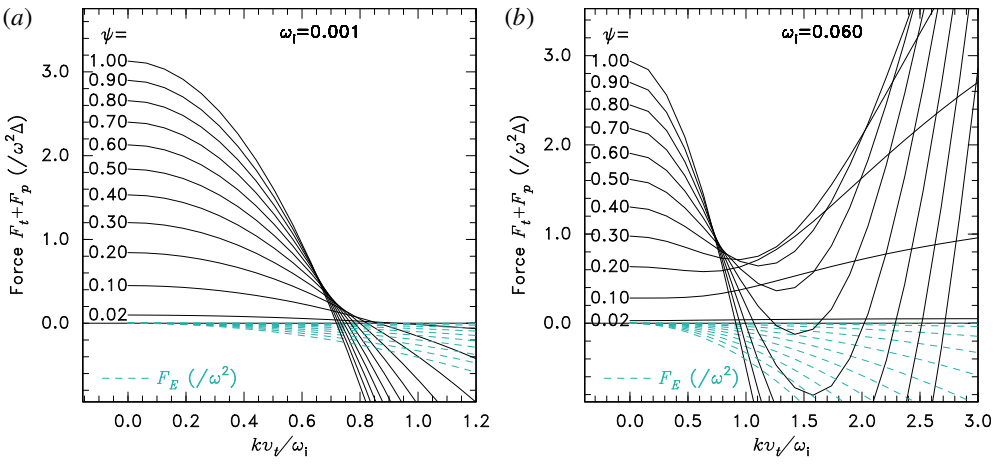

FIGURE 3. Total particle force $F_t + F_p$, and electric force F_E, normalized to ω^2 versus wavenumber k. The dispersion relation is $F_t + F_p = F_E$.

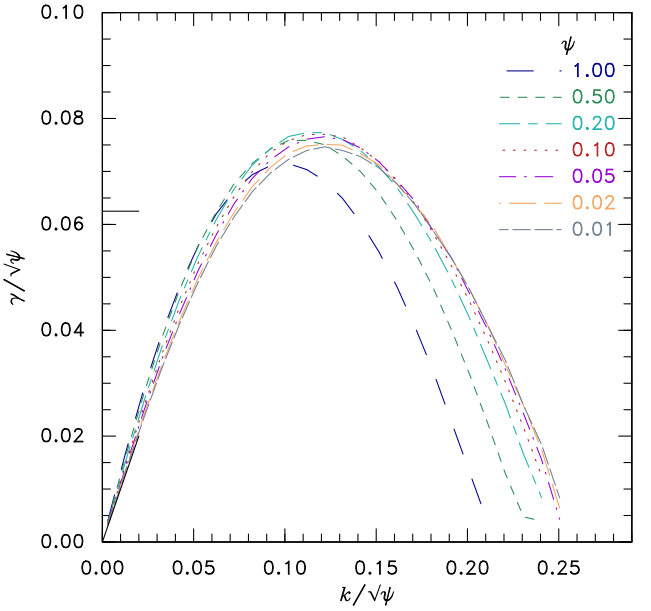

FIGURE 4. Dispersion relation showing scaled transverse instability growth rate versus scaled transverse wavenumber, for a wide range of hole potential ψ. Stationary hole, $\phi = \psi \operatorname{sech}^4(z/4)$, Maxwellian background, immobile ions. Units of γ, z (and k^{-1}) and ψ are respectively ω_p, λ_{De} and T_e/e.

(Here and subsequently in presenting numerical results we use non-dimensionalized parameters where units of time are $1/\omega_p$, of space λ_D and of energy T_e/e; that is equivalent to setting $|q_e| = m_e = 1$.) The iterative numerical solution breaks down at the upper end of the k-range (k_c) where ω_i returns to zero, because the integrals no longer converge. Numerically it breaks down just before k_c, because of imprecision; that is why the curves do not extend all the way back to the k axis. The forces are

https://doi.org/10.1017/S0022377818000909 Published online by Cambridge University Press

evaluated using the same first-order approximation for β which is inaccurate at $\psi \sim 1$. That is one reason why the curves only become truly invariant at low ψ. Another is that F_E begins to become significant for $\psi \sim 1$. Observe that the slope at the origin also somewhat exceeds the limit value of 1 (indicated by the short solid line) except when $\psi \ll 1$. That is consistent with (4.27). The peak growth rate occurs very close to the previously published (Hutchinson 2018) estimate $k = \sqrt{\psi}/8$. The maximum growth rate, even at low ψ somewhat exceeds the prior estimate $\gamma/\sqrt{\psi} = 1/16$. This section has thus confirmed that the transverse instability of electron holes (in Maxwellian background plasma) is a kinematic effect arising from the jetting force balance in an accelerating hole; and it has given a detailed mathematical derivation and precise numerical evaluation of coefficients.

5. Magnetized holes

In the presence of a magnetic field (in the z-direction), the unperturbed orbit is a helix. Because v_z is not constant, the helix has varying pitch, but since the wave vector is perpendicular to B, that does not matter. Take the perpendicular components of velocity at time t to be $v_x(t) = v_\perp \cos\theta_t$ and $v_y(t) = v_\perp \sin\theta_t$, and write $\Omega = eB/m_e$ ($q_e = -e$ so rotation is right-handed about z for positive B). Then at a different time τ, the orbit is

$$\left.\begin{array}{c} v_x(\tau) = v_\perp \cos(\theta_t + \Omega[\tau - t]), \quad v_y(\tau) = v_\perp \sin(\theta_t + \Omega[\tau - t]), \\ x(\tau) = x_t + (v_\perp/\Omega)\{\sin(\theta_t + \Omega[\tau - t]) - \sin\theta_t\}, \\ y(\tau) = y_t + (v_\perp/\Omega)\{-\cos(\theta_t + \Omega[\tau - t]) + \cos\theta_t\}. \end{array}\right\} \tag{5.1}$$

We substitute the orbit parameters into the integral (2.7) and evaluate it. The exponential's argument becomes

$$\mathrm{i}\{ky_t + \xi(\cos\theta_t - \cos[\theta_t + \Omega(\tau - t)]) - \omega\tau\}, \tag{5.2}$$

where $\xi = kv_\perp/\Omega$. We can then write the τ-dependence using the Fourier expansion

$$\mathrm{e}^{-\mathrm{i}\xi\cos\theta_\tau} = \sum_{m=-\infty}^{\infty} \mathrm{e}^{-\mathrm{i}m\theta_\tau}(-\mathrm{i})^m \mathrm{J}_m(\xi), \tag{5.3}$$

(and its derivative with respect to the variable $\theta_\tau = \theta_t + \Omega(\tau - t)$). From which we find

$$\mathrm{e}^{\mathrm{i}(ky_\tau - \omega\tau)} = \sum_m (-\mathrm{i})^m \mathrm{J}_m(\xi)\mathrm{e}^{-\mathrm{i}(m\theta_t - \xi\cos\theta_t)}\mathrm{e}^{\mathrm{i}(ky_t + m\Omega t)}\mathrm{e}^{-\mathrm{i}(m\Omega+\omega)\tau} \tag{5.4}$$

and

$$(kv_\perp/\Omega)\sin\theta_\tau \mathrm{e}^{\mathrm{i}(ky_\tau - \omega\tau)} = -\sum_m m(-\mathrm{i})^m \mathrm{J}_m(\xi)\mathrm{e}^{-\mathrm{i}(m\theta_t - \xi\cos\theta_t)}\mathrm{e}^{\mathrm{i}(ky_t + m\Omega t)}\mathrm{e}^{-\mathrm{i}(m\Omega+\omega)\tau}. \tag{5.5}$$

Everything can be taken outside the τ-integral for $\tilde{f}$, except the final exponential and the quantity $\hat{\phi}(z(\tau))$. So we define the following quantity, which is independent of t (but not $z(t)$),

$$\Phi_m(z) \equiv \int_{-\infty}^{t} \hat{\phi}(z(\tau))\mathrm{e}^{-\mathrm{i}(m\Omega+\omega)(\tau - t)}\,\mathrm{d}\tau, \tag{5.6}$$

https://doi.org/10.1017/S0022377818000909 Published online by Cambridge University Press

where $z(\tau) = z(t) + \int_t^\tau v_z(t')\,\mathrm{d}t'$. The quantity Φ_m is a partial-domain Fourier transform of $\hat{\phi}(z(\tau))$ corresponding to cyclotron harmonic m. It also has exactly the same form as the unmagnetized $\Phi(z)$ with the identification $\omega' = \omega + m\Omega$ (instead of $\omega' = \omega - kv_y$). The remaining space and time t-dependence of $\tilde{f}$ (2.8) is then contained in a term $\mathrm{e}^{\mathrm{i}(ky_t+\omega t)}$. The dependence on the gyrophase angle at time t, θ_t, is specified by the velocity $\boldsymbol{v}$ in the argument of $f_1(\boldsymbol{v}, \boldsymbol{x}, t)$. The quantities we need to evaluate, such as the density and force, require us to integrate over all $\boldsymbol{v}$, which we can begin to do by integrating over θ_t. In view of the Bessel function Fourier expansions, we can write

$$\mathrm{e}^{-\mathrm{i}(m\theta_t - \xi\cos\theta_t)} = \sum_{\ell=-\infty}^{\infty} \mathrm{i}^\ell \mathrm{e}^{\mathrm{i}(\ell-m)\theta_t} \mathrm{J}_\ell(\xi) \tag{5.7}$$

which when integrated over θ_t gives $2\pi\mathrm{i}^m\mathrm{J}_\ell(\xi)$ when $\ell = m$, but zero otherwise. (Everything else in the $\tilde{f}$ integral is independent of θ_t.) Consequently (dropping the t suffix as indication of the final orbit position now, so we can use it instead to denote thermal)

$$\int \tilde{f}\,\mathrm{d}\theta/2\pi = \mathrm{i}\sum_m \left[(m\Omega+\omega)\frac{\partial f_0}{\partial W_\parallel} - m\Omega\frac{\partial f_0}{\partial W_\perp}\right] q_e\Phi_m \mathrm{J}_m^2(\xi)\mathrm{e}^{\mathrm{i}(ky-\omega t)}. \tag{5.8}$$

If the perpendicular distribution is Maxwellian $f_{\perp 0} = (m_e/2\pi T_\perp)\exp(-W_\perp/T_\perp)$, then the integral with respect to $v_\perp$ is analytic $\int_0^\infty \mathrm{J}_m^2(\xi) v_\perp f_{\perp 0}\,\mathrm{d}v_\perp = \exp(-\xi_t^2)\mathrm{I}_m(\xi_t^2)/2\pi$, where $\xi_t^2 = k^2T_\perp/\Omega^2 m_e$, and I_m is the modified Bessel function. Also $\partial f_{\perp 0}/\partial W_\perp = -f_{\perp 0}/T_\perp$. Then there results an expression for the perturbed parallel distribution function

$$f_{\parallel 1}(y,t) = q_e\phi_1(t)\left.\frac{\partial f_{\parallel 0}}{\partial W_\parallel}\right|_t + \sum_m \mathrm{i}\left[(m\Omega+\omega)\frac{\partial f_{\parallel 0}}{\partial W_\parallel} + m\Omega\frac{f_{\parallel 0}}{T_\perp}\right] q_e\Phi_m \mathrm{e}^{-\xi_t^2}\mathrm{I}_m(\xi_t^2)\mathrm{e}^{\mathrm{i}(ky-\omega t)}. \tag{5.9}$$

We naturally denote the second term (the sum) as $\tilde{f}_\parallel \mathrm{e}^{\mathrm{i}(ky-\omega t)}$.

With this expression we have replaced the integral over perpendicular velocities that was necessary for the unmagnetized case with a sum over $\Phi_m \mathrm{e}^{-\xi_t^2}\mathrm{I}_m(\xi_t)$. Therefore the numerical effort involved in evaluating the force is no greater than what is needed to evaluate the zero field case by numerical integration over the perpendicular distribution (although it is limited to Gaussian perpendicular distributions). Moreover, Φ_m is essentially exactly the same quantity as the unmagnetized Φ. Regarding $\Phi(z, \omega', W_\parallel)$ as a function of z and ω', straightforwardly $\Phi_m(z) = \Phi(z, \omega + m\Omega, W_\parallel)$; with $\omega' \to \omega + m\Omega$ (instead of $\omega - kv_y$). The close connection to the unmagnetized calculation can be understood by plotting $\xi_t \mathrm{e}^{-\xi_t^2}\mathrm{I}_m(\xi_t^2)$ versus the transverse phase velocity of harmonic m as shown in figure 5. Harmonics are spaced by a velocity increment (in units of the thermal velocity $v_t = \sqrt{T_\perp/m_e}$) that is $\delta v = 1/\xi_t = \Omega/kv_t$. Consequently the sum $\sum_m \mathrm{e}^{-\xi_t^2}\mathrm{I}_m(\xi_t^2) = \sum_m \xi_t \mathrm{e}^{-\xi_t^2}\mathrm{I}_m(\xi_t^2)\delta v$, when $\xi_t > 1$, represents a kind of finite-difference approximation to the integral $\int \xi_t \mathrm{e}^{-\xi_t^2}\mathrm{I}_m(\xi_t^2)\,\mathrm{d}v_m$, where $v_m = m/\xi_t$ is regarded as a continuous variable for given ξ_t. Figure 5 shows how quickly the values of the harmonic sum approximates the integral over a Gaussian perpendicular velocity distribution as the magnetic field becomes smaller.

https://doi.org/10.1017/S0022377818000909 Published online by Cambridge University Press

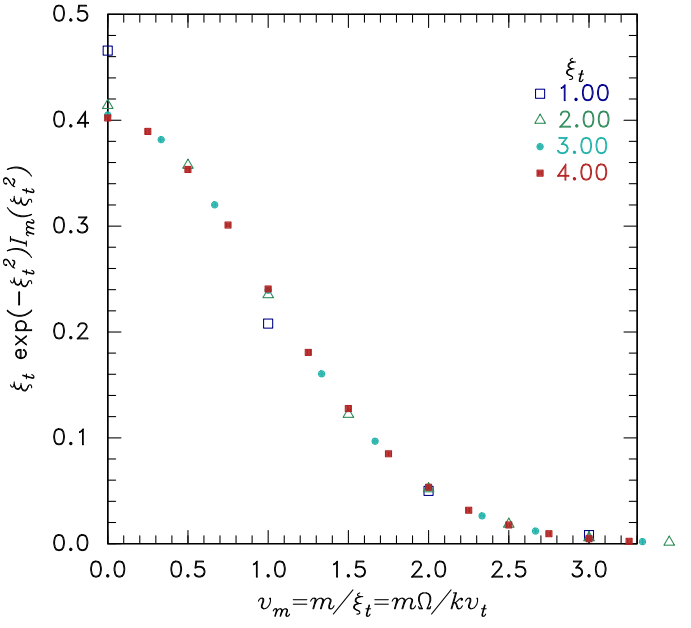

FIGURE 5. Illustration of the Bessel function harmonic sum approximating a transverse Maxwellian distribution.

At low values of $\xi_t(<1)$ (high magnetic field), only one or two harmonics give any substantial contribution. In the infinite-field limit, when only the $m=0$ harmonic matters (and $\mathrm{I}_0(0)=1$), we return to the one-dimensional motion expression:

$$f_{\parallel 1}(t) = q_e\phi_1(t)\left.\frac{\partial f_{\parallel 0}}{\partial W_\parallel}\right|_t + \mathrm{i}\omega\frac{\partial f_{\parallel 0}}{\partial W_\parallel} q_e\Phi_0 \mathrm{e}^{\mathrm{i}(ky_t-\omega t)}, \tag{5.10}$$

which amounts to setting effectively $k=0$. As Ω is decreased from infinity (ξ_t raised from zero), the $m=\pm 1$ terms next become important. And for $\xi_t \ll 1$, since $\mathrm{e}^{-\xi_t^2}\mathrm{I}_m(\xi_t^2) \simeq (\xi_t^2/2)^m/m!$, the higher-$m$ terms are negligible (although up to at least $m=4$ are kept in the numerics to retain precision). Noting $\Phi(\omega') = (m_e\Delta/q_e)\omega'\tilde{L}(\omega')$, in (5.9) the $m=1$ relevant coefficient for small ω is $m\Omega\Phi_m \mathrm{e}^{-\xi_t^2}\mathrm{I}_m(\xi_t^2) = (m_e\Delta/q_e)\tilde{L}\Omega^2\xi_t^2/2 = (m_e\Delta/q_e)\tilde{L}k^2v_t^2/2$, whose only dependence on Ω enters through $\tilde{L}(\omega')$, that is through finite transit time effects. The particle force becomes

$$\begin{aligned}\tilde{F} &= -\mathrm{i}\int q_e\frac{\mathrm{d}\phi_0}{\mathrm{d}z}\left[\frac{\partial f_{\parallel 0}}{\partial W_\parallel}\omega\sum_{m=0,\pm 1}[\Phi_m \mathrm{e}^{-\xi_t^2}\mathrm{I}_m(\xi_t^2)]\right.\\ &\quad\left.+\left(\frac{\partial f_{\parallel 0}}{\partial W_\parallel}+\frac{f_{\parallel 0}}{T_\perp}\right)\sum_{m=\pm 1} m\Omega[\Phi_m \mathrm{e}^{-\xi_t^2}\mathrm{I}_m(\xi_t^2)]\right]\mathrm{d}v_z\,\mathrm{d}z\\ &\simeq -m_e\Delta\int q_e\frac{\mathrm{d}\phi_0}{\mathrm{d}z}\left[\frac{\partial f_{\parallel 0}}{\partial W_\parallel}\omega^2\mathrm{i}\tilde{L}(\omega)+\frac{\partial f_{\parallel t}}{\partial W_\parallel}\left(1+\frac{1}{|\beta|}\right)\frac{1}{2}k^2v_t^2\sum_{\pm 1}\mathrm{i}\tilde{L}(m\Omega+\omega)\right]\mathrm{d}v_z\,\mathrm{d}z,\end{aligned} \tag{5.11}$$

https://doi.org/10.1017/S0022377818000909 Published online by Cambridge University Press

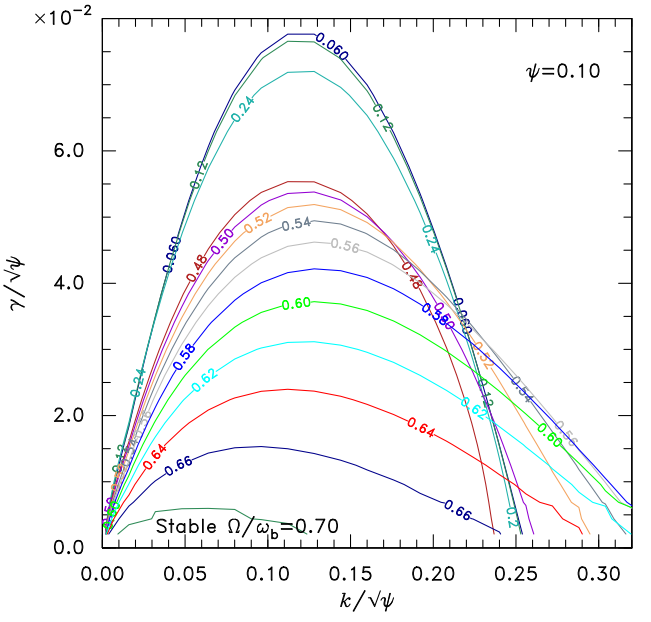

FIGURE 6. The zero contours of $F_p + F_t - F_E$ for magnetized holes labelled with the increasing values of Ω/ω_b. The contours give the dispersion relation $\gamma(k)$. Magnetic stabilization of the transverse instability occurs as $\Omega/\omega_b \simeq 0.7$ is approached.

where terms of order ω/Ω and higher are neglected, $\partial f_{\|t}/\partial W_\|$ denotes the trapped distribution's slope, and the passing $m = \pm 1$ contribution cancels by isotropy. This is identical to (4.22) except insofar as the argument of $\tilde{L}$ is changed. Since $\tilde{L}$ is constant in the short transit time limit, instability there is not stabilized by magnetic field. The low-k instability growth rate is still positive and given by (4.27) unless Ω is at least of order the predominant bounce frequency ω_b, so as to change $\tilde{L}(\Omega + \omega)$. For definiteness we take $\omega_b = \sqrt{\psi}/2$, which is the (dimensionless) bounce frequency in a $\psi\,\mathrm{sech}^4 z/4$ hole for trapped particles at the bottom of the potential energy well.

What is required for stabilization is that (for small $\omega = \mathrm{i}\omega_i$) the value (which is real) of $\sum_{m=\pm1} \int \mathrm{i}\tilde{L}(m\Omega + \mathrm{i}\omega_i)(\mathrm{d}\phi_0/\mathrm{d}z)\,\mathrm{d}z(\mathrm{d}f_{\|t}/\mathrm{d}W_\|)\,\mathrm{d}v_z$, for trapped particles be reversed, or else reduced sufficiently that the combination with the electric field tension is reversed, so that the dispersion relation $\tilde{F}_p = -\tilde{F}_t + F_E$ cannot be satisfied.

The total consequence of magnetization can be conveniently documented by creating a contour plot of the total force $\tilde{F}_t + \tilde{F}_p - F_E$ over the relevant domain of $\omega_i = \gamma$ and k. The sum of cyclotron harmonics replaces the $\int \mathrm{d}v_y$ and is used to evaluate the force for the entire hole. Only the zero contour of a series of contour plots for different Ω is shown in figure 6, since zero value occurs at the solution of the dispersion relation (when there is one). The labels are the values of Ω/ω_b. Once again, this is a nearly universal figure for the $\mathrm{sech}^4(z/4)$ hole, at least at low ψ where the β approximation for the trapped energy distribution is accurate.

Stabilization arises from a reversal of $\tilde{F}_t$, which can be understood by examining the contributions to the trapped force from different trapped energy particles. Figure 7 shows how the contribution to trapped force from different parallel energy orbits varies for different real parts (ω_r) of ω' in (4.32). It is expressed as $\mathrm{d}F_t/\mathrm{d}(-W_\|)^{1/2}$ versus $(-W_\|)^{1/2}$, so that the total force is the area under the curve, integrated from

https://doi.org/10.1017/S0022377818000909 Published online by Cambridge University Press

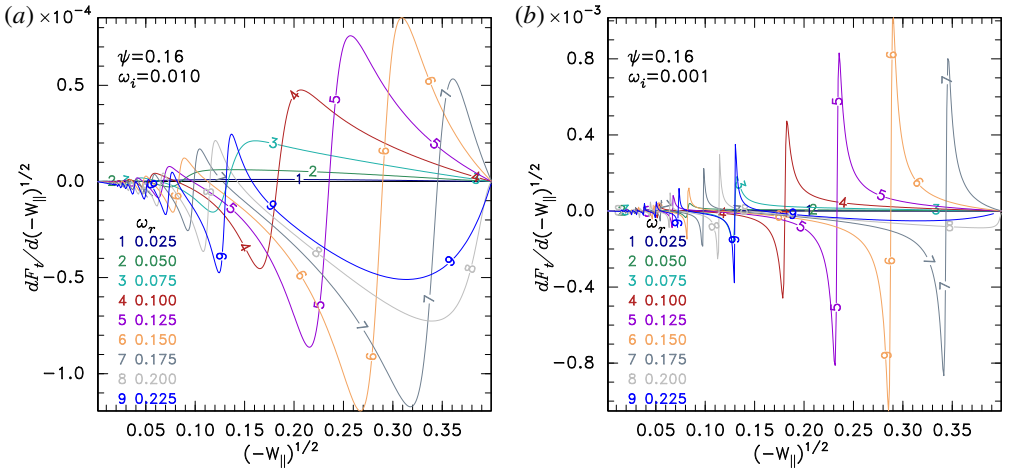

FIGURE 7. Contributions to the trapped particle force for specific real and imaginary parts of ω', as a function of trapped energy. The real part ω_r corresponds to Ω. The effects of bounce resonances dominate the variation at higher ω_r. Resonances are sharper at lower ω_i, (*b*), than at higher, (*a*).

zero to $\sqrt{\psi}$ (the right-hand end). The application to a magnetized case is that the cyclotron harmonic trapped force contribution is equal to the same integral but with $\omega_r = \Omega$. So this plot represents how the $(m = \pm 1)$ trapped force depends on parallel energy. The behaviour is dominated by resonances between the frequency ω_r and the bounce frequency of the particles (and its harmonics, since the bounce orbits are anharmonic). The bounce frequency varies from zero for marginally trapped particles $(W_\parallel = 0)$ to the value $\omega_b = \sqrt{\psi}/2$ for the deepest trapped particles $-W_\parallel = \psi$. The resonant energy corresponds to the place where the curve passes rapidly through zero. For the unmagnetized case, contributions for $kv_y = \omega_r$ are represented by the same plot.

Low ω_r is resonant only at very low bounce frequency, which means low $|W_\parallel|$: marginally trapped particles at the left-hand end of the plot. Thus the areas under curves 1 and 2 in figure 7(*a*) are dominated by regions to the right of the resonances, where $\mathrm{d}F_t/\mathrm{d}(-W)^{1/2}$ is positive. Curves 3 and 4 show the fundamental resonance approaching the centre of the energy range; so significant contribution is beginning to arise from regions to the left of the fundamental resonance where $\mathrm{d}F_t/\mathrm{d}(-W)^{1/2}$ is negative. Curves 5 and 6 show the transition to the state where the negative contributions exceed the positive, and curve 8 corresponds to $\omega_r = \sqrt{\psi}/2$ where the resonance is exactly at the right-hand end of the energy range: particles at the bottom of the potential well. It has a clearly predominant negative integrated force. For the higher frequencies, e.g. 8 and 9, it is easy to see the second (and higher) bounce-frequency harmonic resonance effects in the left-hand one third of the energy range.

All these qualitative statements depend little on the choice of other parameters. The hole depth ψ determines the energy range of the plot; the imaginary part of ω', ω_i, determines the sharpness of the resonance, as is seen by comparing figures 7(*a*) with 7(*b*). Low ω_i requires fine energy mesh to resolve accurately. Once $\omega_r > \omega_b$ the first bounce harmonic resonance disappears but stability remains, showing that cyclotron damping *per se* is not the stabilization mechanism, since no particles are then resonant.

https://doi.org/10.1017/S0022377818000909 Published online by Cambridge University Press

6. Summary

The transverse instability of an electron hole in an isotropic Maxwellian background plasma arises not because of orbit transverse 'focusing' but because of the overall hole force balance arising from the kinematic parallel jetting (energization) of particles. The shift mode is the relevant low-frequency perturbation eigenmode, proportional to the spatial derivative of the hole potential. It is demonstrated that a linearized Vlasov–Poisson calculation of the jetting force gives expressions identical at low frequency to those recently derived by more elementary analysis. Previous stability analyses of symmetric eigenmodes are irrelevant to the long-wavelength shift mode which kinks the hole, because the shift mode is antisymmetric. A rigorous linear analysis of the dispersion relation of the shift mode has been completed for a slowly moving electron hole, ignoring ion motion. The instability is purely growing and $\gamma(k)$ has been found and expressed in essentially universal form (figure 4). The peak growth rate occurs, for a $\psi\,\mathrm{sech}^4(z/4\lambda_D)$ hole potential, at $k\lambda_D \simeq \sqrt{e\psi/T_e}/8$, with a value (in the absence of magnetic field) slightly above $\gamma = \omega_p\sqrt{e\psi/T_e}/16$, in good confirmation of the recent estimates (Hutchinson 2018) based on the same kinematic mechanism. The magnetized case has also been analysed (figure 6), showing that stabilization occurs at $\Omega \simeq 0.7\omega_b$ where $\omega_b = \omega_p\sqrt{e\psi/T_e}/2$ is the bounce frequency of deeply trapped electrons. Stabilization occurs because the jetting force on the trapped electrons reverses its sign across the resonance between the bounce and cyclotron frequencies (figure 7). The same sort of reversal effect is responsible for suppressing the unmagnetized instability when $kv_t \gtrsim \omega_b$. This upper k-limit suggests that holes with transverse extent less than approximately $4\pi\lambda_D\sqrt{T_e/e\psi}$ should not suffer this instability. As (4.27) shows, it is the transverse temperature T_y that determines the low-k growth rate. Particle-in-cell simulations observe that the transverse temperature can alter the observed growth rate, but have not yet established the dependence systematically enough to test the analytical prediction.

There remain some discrepancies between the present analysis and simulation observations. In Maxwellian plasmas it has been documented in Hutchinson (2018) that a higher magnetic field $\Omega \simeq 1.5\sqrt{\psi}/2$ than predicted here is needed for complete stability. That might perhaps be explained by the simulation potential being more peaked than $\mathrm{sech}^4(z/4\lambda_D)$ or by trapped electron distributions differing from the negative-temperature Maxwellian form used here. But it might also indicate a shortcoming in the assumption made here that the eigenmode is a pure shift mode. It is possible that a distorted or more complicated mode might remain less stable near the shift mode's marginal stability.

Simulations with non-Maxwellian background plasma (Goldman *et al.* 1999; Oppenheim *et al.* 1999; Newman *et al.* 2001; Oppenheim *et al.* 2001; Berthomier *et al.* 2002; Lu *et al.* 2008; Wu *et al.* 2010) have also observed instabilities of different character and shorter y-wavelength even above this higher-field stability limit. And holes of limited transverse dimensions are observed by spacecraft even in regions where $\Omega > \omega_b$, as well as in lower magnetic field regions. These facts are not explained by the current transverse instability analysis. Maxwellian shape $f(v)$ was deliberately chosen here to give an unequivocally stable background and rule out instability enhancement by the untrapped background. The present analysis can readily be extended to address such cases as anisotropic bi-Maxwellians. In any case, the 'whistler' or 'streaked' instabilities observed at high magnetic field in codes are not pure shift modes, and probably require different assumptions about eigenstructure, such as those of Vetoulis & Oppenheim (2001).

https://doi.org/10.1017/S0022377818000909 Published online by Cambridge University Press

Acknowledgements

I am grateful to C. Zhou for our many thoughtful discussions of electron hole kinematics, and to the anonymous reviewer of a previous paper who alerted us to the ideas in § 3.1. X. Chen helped by checking some of the algebra. This work was partially supported by NASA grant NNX16AG82G.

REFERENCES

ANDERSSON, L., ERGUN, R. E., TAO, J., ROUX, A., LECONTEL, O., ANGELOPOULOS, V., BONNELL, J., MCFADDEN, J. P., LARSON, D. E., ERIKSSON, S. *et al.* 2009 New features of electron phase space holes observed by the THEMIS mission. *Phys. Rev. Lett.* **102** (22), 225004.

BALE, S. D., KELLOGG, P. J., LARSEN, D. E., LIN, R. P., GOETZ, K. & LEPPING, R. P. 1998 Bipolar electrostatic structures in the shock transition region: evidence of electron phase space holes. *Geophys. Res. Lett.* **25** (15), 2929–2932.

BERNSTEIN, I. B., GREENE, J. M. & KRUSKAL, M. D. 1957 Exact nonlinear plasma oscillations. *Phys. Rev.* **108** (4), 546–550.

BERTHOMIER, M., MUSCHIETTI, L., BONNELL, J. W., ROTH, I. & CARLSON, C. W. 2002 Interaction between electrostatic whistlers and electron holes in the auroral region. *J. Geophys. Res.* **107** (A12), 1–11.

ELIASSON, B. & SHUKLA, P. K. 2006 Formation and dynamics of coherent structures involving phase-space vortices in plasmas. *Phys. Rep.* **422** (6), 225–290.

ERGUN, R. E., CARLSON, C. W., MCFADDEN, J. P., MOZER, F. S., MUSCHIETTI, L., ROTH, I. & STRANGEWAY, R. J. 1998 Debye-scale plasma structures associated with magnetic-field-aligned electric fields. *Phys. Rev. Lett.* **81** (4), 826–829.

GOLDMAN, M. V., OPPENHEIM, M. M. & NEWMAN, D. L. 1999 Nonlinear two-stream instabilities as an explanation for auroral bipolar wave structures. *Geophys. Res. Lett.* **26** (13), 1821–1824.

HUTCHINSON, I. H. 2017 Electron holes in phase space: What they are and why they matter. *Phys. Plasmas* **24** (5), 055601.

HUTCHINSON, I. H. 2018 On the mechanism of plasma electron hole transverse instability. *Phys. Rev. Lett.* **120** (20), 205101.

HUTCHINSON, I. H. & ZHOU, C. 2016 Plasma electron hole kinematics. I. Momentum conservation. *Phys. Plasmas* **23** (8), 82101.

JOVANOVIĆ, D. & SCHAMEL, H. 2002 The stability of propagating slab electron holes in a magnetized plasma. *Phys. Plasmas* **9** (12), 5079–5087.

LEWIS, H. R. & SEYLER, C. 1982 Stability of Vlasov Equilibria. Part 2. One ignorable coordinate. *J. Plasma Phys.* **27**, 25–35.

LEWIS, H. R. & SYMON, K. R. 1979 Linearized analysis of inhomogeneous plasma equilibria: general theory. *J. Math. Phys.* **20** (1979), 413.

LU, Q. M., LEMBEGE, B., TAO, J. B. & WANG, S. 2008 Perpendicular electric field in two-dimensional electron phase-holes: a parameter study. *J. Geophys. Res.* **113** (A11), A11219.

MALASPINA, D. M., ANDERSSON, L., ERGUN, R. E., WYGANT, J. R., BONNELL, J. W., KLETZING, C., REEVES, G. D., SKOUG, R. M. & LARSEN, B. A. 2014 Nonlinear electric field structures in the inner magnetosphere. *Geophys. Res. Lett.* **41**, 5693–5701.

MALASPINA, D. M., NEWMAN, D. L., WILLSON, L. B., GOETZ, K., KELLOGG, P. J. & KERSTIN, K. 2013 Electrostatic solitary waves in the solar wind: evidence for instability at solar wind current sheets. *J. Geophys. Res.* **118** (2), 591–599.

MANGENEY, A., SALEM, C., LACOMBE, C., BOUGERET, J.-L., PERCHE, C., MANNING, R., KELLOGG, P. J., GOETZ, K., MONSON, S. J. & BOSQUED, J.-M. 1999 WIND observations of coherent electrostatic waves in the solar wind. *Ann. Geophys.* **17** (3), 307–320.

MATSUMOTO, H., KOJIMA, H., MIYATAKE, T., OMURA, Y., OKADA, M., NAGANO, I. & TSUTSUI, M. 1994 Electrostatic solitary waves (ESW) in the magnetotail: BEN wave forms observed by GEOTAIL. *Geophys. Res. Lett.* **21** (25), 2915–2918.

MIYAKE, T., OMURA, Y., MATSUMOTO, H. & KOJIMA, H. 1998 Two-dimensional computer simulations of electrostatic solitary waves observed by Geotail spacecraft. *J. Geophys. Res.* **103** (A6), 11841.

MORSE, R. L. & NIELSON, C. W. 1969 One-, two-, and three-dimensional numerical simulation of two-beam plasmas. *Phys. Rev. Lett.* **23** (19), 1087–1090.

MOTTEZ, F., PERRAUT, S., ROUX, A. & LOUARN, P. 1997 Coherent structures in the magnetotail triggered by counterstreaming electron beams. *J. Geophys. Res.* **102** (A6), 11399.

MOZER, F. S., AGAPITOV, O. A., ARTEMYEV, A., BURCH, J. L., ERGUN, R. E., GILES, B. L., MOURENAS, D., TORBERT, R. B., PHAN, T. D. & VASKO, I. 2016 Magnetospheric multiscale satellite observations of parallel electron acceleration in magnetic field reconnection by Fermi reflection from time domain structures. *Phys. Rev. Lett.* **116** (14), 4–8.

MUSCHIETTI, L., ROTH, I., CARLSON, C. W. & ERGUN, R. E. 2000 Transverse instability of magnetized electron holes. *Phys. Rev. Lett.* **85** (1), 94–97.

MUSCHIETTI, L., ROTH, I., ERGUN, R. E. & CARLSON, C. W. 1999 Analysis and simulation of BGK electron holes. *Nonlinear Process. Geophys.* **6** (3/4), 211–219.

NEWMAN, D. L., GOLDMAN, M. V., SPECTOR, M. & PEREZ, F. 2001 Dynamics and instability of electron phase-space tubes. *Phys. Rev. Lett.* **86** (7), 1239–1242.

OPPENHEIM, M., NEWMAN, D. L. & GOLDMAN, M. V. 1999 Evolution of electron phase-space holes in a 2D magnetized plasma. *Phys. Rev. Lett.* **83** (12), 2344–2347.

OPPENHEIM, M. M., VETOULIS, G., NEWMAN, D. L. & GOLDMAN, M. V. 2001 Evolution of electron phase-space holes in 3D. *Geophys. Res. Lett.* **28** (9), 1891–1894.

PICKETT, J. S., CHEN, L.-J., MUTEL, R. L., CHRISTOPHER, I. W., SANTOLK, O., LAKHINA, G. S., SINGH, S. V., REDDY, R. V., GURNETT, D. A., TSURUTANI, B. T. *et al.* 2008 Furthering our understanding of electrostatic solitary waves through Cluster multispacecraft observations and theory. *Adv. Space Res.* **41** (10), 1666–1676.

SCHAMEL, H. 1979 Theory of electron holes. *Phys. Scr.* **20** (3–4), 336–342.

SCHAMEL, H. 1982 Stability of electron vortex structures in phase space. *Phys. Rev. Lett.* **48** (7), 481–483.

SCHAMEL, H. 1986 Electrostatic phase space structures in theory and experiment. *Phys. Rep.* **3** (3), 161–191.

SCHAMEL, H. 1987 On the stability of localized electrostatic structures. *Z. Naturforsch.* **42a**, 1167–1174.

SINGH, N., LOO, S. M. & WELLS, B. E. 2001 Electron hole structure and its stability depending on plasma magnetization. *J. Geophys. Res.* **106** (A10), 21183–21198.

SKRYABIN, D. V. 2002 Energy of the soliton internal modes and broken symmetries in nonlinear optics. *J. Opt. Soc. Am.* B **19** (3), 529–536.

TURIKOV, V. A. 1984 Electron phase space holes as localized BGK solutions. *Phys. Scr.* **30** (1), 73–77.

VASKO, I. Y., AGAPITOV, O. V., MOZER, F., ARTEMYEV, A. V. & JOVANOVIC, D. 2015 Magnetic field depression within electron holes. *Geophys. Res. Lett.* **42** (7), 2123–2129.

VETOULIS, G. & OPPENHEIM, M. 2001 Electrostatic mode excitation in electron holes due to wave bounce resonances. *Phys. Rev. Lett.* **86** (7), 1235–1238.

WILSON, L. B., CATTELL, C. A., KELLOGG, P. J., GOETZ, K., KERSTEN, K., KASPER, J. C., SZABO, A. & WILBER, M. 2010 Large-amplitude electrostatic waves observed at a supercritical interplanetary shock. *J. Geophys. Res.* **115** (12), A12104.

WU, M., LU, Q., HUANG, C. & WANG, S. 2010 Transverse instability and perpendicular electric field in two-dimensional electron phase-space holes. *J. Geophys. Res.* **115** (10), A10245.

ZHOU, C. & HUTCHINSON, I. H. 2016 Plasma electron hole kinematics. II. Hole tracking particle-in-cell simulation. *Phys. Plasmas* **23** (8), 82102.

ZHOU, C. & HUTCHINSON, I. H. 2017 Plasma electron hole ion-acoustic instability. *J. Plasma Phys.* **83**, 90580501.